Drug Design, Development and Therapy

Dovepress
Taylor & Francis Group

Open Access Full Text Article

ORIGINAL RESEARCH

Effect and Mechanism of Aloin in Ameliorating Chronic Prostatitis/Chronic Pelvic Pain Syndrome: Network Pharmacology and Experimental Verification

Rongxin Li[1–3], Yanan Wang[1–3], Yongfeng Lao[1–3], Chengyu You[1–3], Liangliang Qing[1–3], Xin Guan[1–3], Jian Wang[1–3], Xiaolong Li[1–3], Qingchao Li[1–3], Shuai Liu[1–3], Zhilong Dong[1–3]

[1]Department of Urology, The Second Hospital of Lanzhou University, Lanzhou, Gansu, 730000, People's Republic of China; [2]Gansu Province Key Laboratory of Urological Diseases, Lanzhou, Gansu, 730030, People's Republic of China; [3]Gansu Province Clinical Research Center for Urinary System Disease, Lanzhou, Gansu, 730000, People's Republic of China

Correspondence: Zhilong Dong, Department of Urology, The Second Hospital of Lanzhou University, 82, Cuiyingmen, Chengguan District, Lanzhou, Gansu Province, People's Republic of China, Email dzl19780829@163.com

Purpose: This research aims to investigate the role and potential mechanisms of Aloin in Chronic Prostatitis/Chronic Pelvic Pain Syndrome (CP/CPPS) through network pharmacology and experimental approaches.

Methods: Using network pharmacology methods, potential targets of Aloin and targets related to CP/CPPS were screened from public databases. The protein-protein interaction (PPI) network, Gene Ontology (GO), and Kyoto Encyclopedia of Genes and Genomes (KEGG) pathway enrichment analysis were performed to predict the core targets and pathways of Aloin against CP/CPPS. The effects of Aloin in ameliorating CP/CPPS were verified in animal experiments.

Results: A total of 235 genes interacting with Aloin in CP/CPPS were identified. PPI network analysis revealed five core targets: AKT1, EGFR, ESR1, HSP90AA1, and SRC. GO analysis yielded 2916 enrichment results, with 2562 related to Biological Process (BP), 94 to Cellular Component (CC), and 260 to Molecular Function (MF). KEGG pathway analysis identified 172 pathways. Molecular docking confirmed stable binding between Aloin and core targets. Molecular dynamics simulations further validated binding stability by analyzing Root Mean Square Deviation (RMSD), Root Mean Square Fluctuation (RMSF), Radius of Gyration (Rg), hydrogen bonds, Solvent Accessible Surface Area (SASA), and Gibbs free energy of Aloin-target complexes. Experimental validation showed that Aloin alleviated pain, reduced inflammatory factors, and decreased oxidative stress in a rat model of CP/CPPS. The qRT-PCR results showed that Aloin intervention reduced the mRNA expression of AKT1, EGFR, HSP90AA1, and SRC, while increasing ESR1 mRNA expression. These changes may underlie its therapeutic effects in CP/CPPS.

Conclusion: Our study revealed that Aloin exerts a beneficial effect on mitigating the pain symptoms associated with CP/CPPS, ameliorating inflammation, and reducing oxidative stress. Through network pharmacology, potential targets and signaling pathways were identified, suggesting the therapeutic promise of Aloin for CP/CPPS. These findings advocate for further exploration into its clinical efficacy and mechanistic underpinnings in the treatment of CP/CPPS.

Keywords: Aloin, chronic prostatitis, CP/CPPS, network pharmacology

Introduction

Chronic Prostatitis/Chronic Pelvic Pain Syndrome (CP/CPPS) is a prevalent urological disorder that significantly impacts men's health and quality of life, which is classified as type III prostatitis by the National Institutes of Health in the United States (NIH).[1] The primary symptoms of CP/CPPS include chronic pelvic pain and urinary symptoms, which may be accompanied by sexual dysfunction and psychosomatic symptoms. CP/CPPS is the most prevalent type of prostatitis, constituting 90–95% of all prostatitis cases and with an estimated prevalence rate of up to 15% among the male population.[2,3] It is characterized by a low

Received: 18 October 2024
Accepted: 3 March 2025
Published: 14 March 2025

cure rate, high recurrence rate, complex symptoms, prolonged course, a wide range of painful sites, and numerous complications, collectively resulting in considerable physical pain and mental burden for patients.[4]

Despite its high prevalence, CP/CPPS remains a condition with unclear etiology. The etiology of CP/CPPS is commonly believed to be associated with infection, chronic inflammation, oxidative stress, immune dysregulation, neuroendocrine issues, and even psychosocial factors.[5–7] Contemporary treatment modalities for CP/CPPS predominantly involve a combination of antibiotics, anti-inflammatory agents, alpha-blockers, and pain management strategies.[8,9] However, these approaches are often only moderately effective, leaving many patients with unresolved symptoms and a diminished quality of life.[10] The elusive nature of CP/CPPS etiology further complicates the development of targeted and effective therapeutic interventions.[10]

Aloin, a bioactive compound derived from Aloe vera, has garnered attention for its potential therapeutic properties, including anti-inflammatory effects.[11] As a member of the anthraquinone compound family, Aloin has been reported to exhibit various biological effects, including anti-tumor, anti-inflammatory, anti-injury, antioxidant, antimicrobial, bone generation, and anti-diabetic effects.[12] Its mechanisms of action may be associated with multiple signaling pathways, such as NF-κB, MAPK, PI3K-AKT, and JAK/STAT, among others. While existing research suggests the anti-inflammatory potential of Aloin, its specific effect on the context of CP/CPPS remains underexplored.

This study aims to investigate the potential targets and mechanisms of Aloin in CP/CPPS using network pharmacology research methods and experimentally validate its effects in animal models (Figure 1).

Materials and Methods

Network Pharmacology Analysis

Target Gene Analysis of Aloin

The target proteins of Aloin were retrieved through SwissTargetPrediction (http://www.swisstargetprediction.ch/), SuperPred (https://prediction.charite.de/), Traditional Chinese Medicine Systems Pharmacology Database and Analysis Platform (TCMSP)(https://www.91tcmsp.com/), and PharmMapper (http://lilab-ecust.cn/pharmmapper/index.html). The obtained target proteins were cross referenced and standardized using data from UniProt (https://www.uniprot.org/). Non-human genes were excluded, and redundant or invalid targets were removed, resulting in a standardized list of gene names.

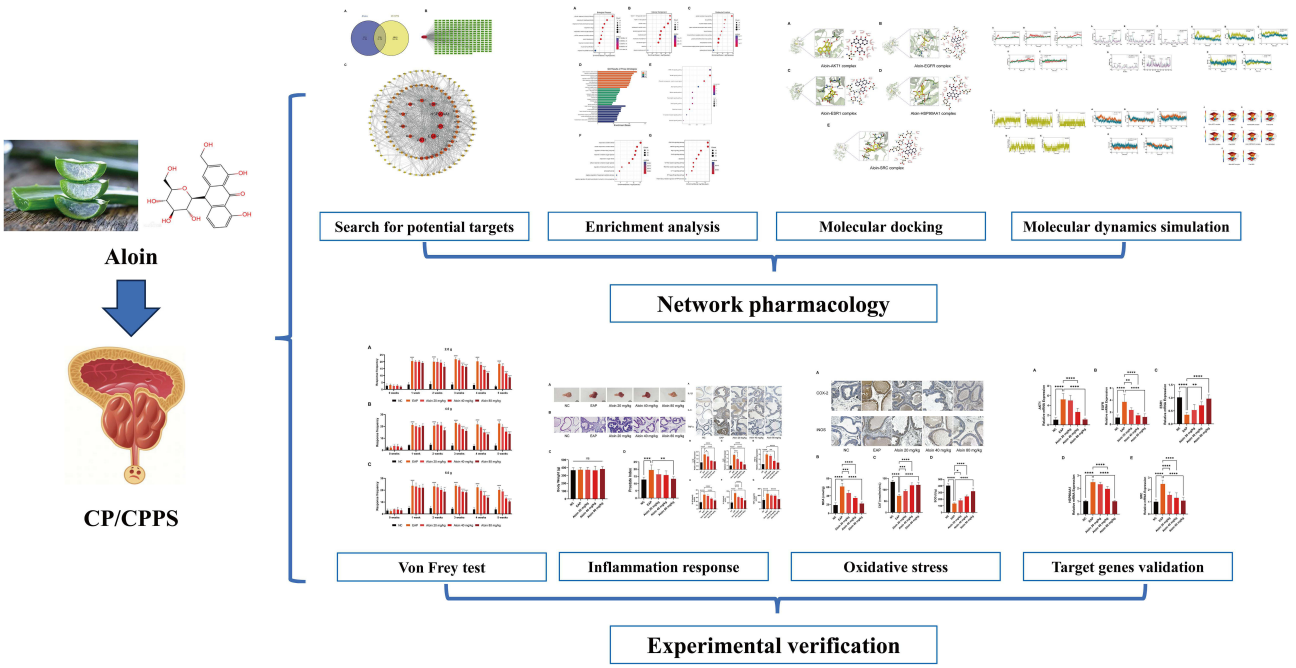

Figure 1 Flowchart of the study design for assessing the effect of Aloin in ameliorating CP/CPPS.

Target Analysis of CP/CPPS

We used "chronic prostatitis with chronic pelvic pain syndrome" as keywords to search and screen disease-related genes in the GeneCards (https://www.genecards.org/), OMIM (https://www.omim.org/), and DisGENET (https://www.disgenet.org/). The obtained Aloin-interacting and disease-related targets were mapped as Venn diagrams to obtain overlapping genes.

Construction of Interaction Network of Aloin Anti-CP/CPPS Target Proteins

To further investigate the interactions between proteins targeted by Aloin for the treatment of CP/CPPS, the overlapping genes were imported into the String database (https://string-db.org/) to construct a Protein-Protein Interaction (PPI) network. The species was set as "Homosapiens", with a minimum interaction score of 0.7 to ensure the reliability of the study. The results were imported into Cytoscape 3.9.1 to map the visual PPI network.

Gene Ontology (GO) and Kyoto Encyclopedia of Genes and Genomes Path (KEGG) Enrichment Analysis

R software version 4.2.1 was utilized for conducting GO enrichment analysis on the overlapping targets. The analysis encompassed three categories: Biological Process (BP), Cellular Component (CC), and Molecular Function (MF). A significance threshold of $p < 0.05$ was applied, and the top ten targets were selected based on their involvement. In addition, KEGG pathway analysis was carried out for the overlapping targets. The selection criteria employed a significance level of $p < 0.05$, and the top 10 signaling pathways were chosen.

Molecular Docking Verification

Targets with the top five degree values were selected as the core targets for molecular docking to verify their interaction activities with Aloin. The structure files of Aloin were retrieved from the PubChem database (https://pubchem.ncbi.nlm.nih.gov/). The 3D structures of core targets of Aloin in CP/CPPS were obtained from the Protein Data Bank (PDB) database (https://www.rcsb.org/). Initially, crystal structures of five core targets, Protein Kinase B (AKT1), Epidermal Growth Factor Receptor (EGFR), Estrogen Receptor 1 (ESR1), Heat Shock Protein 90 Alpha Family Class A Member 1 (HSP90AA1), and Proto-Oncogene c-Src (SRC), were downloaded from the PDB library, including AKT1 (PDB ID: 6NPZ), EGFR (PDB ID: 2GS2), ESR1 (PDB ID: 6SBO), HSP90AA1 (PDB ID: 6U98), and SRC (PDB ID: 2SRC). To ensure the reliability of the PDB structures of the core targets, docking validation was performed using the co-crystal small molecules of each target protein. The applicability of the PDB structures was verified by calculating the root mean square deviation (RMSD) between the docking results and the co-crystal small molecules (Figure S1). The two-dimensional structure of Aloin was then converted into three-dimensional structure using Chembio 3D software. Subsequently, proteins underwent dehydration, hydrogenation, and charge assignment using Auto Dock Tools, followed by molecular docking with Aloin using Autodock Vina 1.1.2. Finally, The molecular visualization was performed using PyMOL 2.3.0 (3D) and Ligplot V2.2.7 (2D) software.

Molecular Dynamics (MD) Simulation

Molecular dynamics simulations of Aloin-protein complexes obtained from molecular docking were performed using GROMACS (version: 2022.03) software. The Amber99sb-ildn force field was employed. The specific steps and parameter settings for the MD simulations are as follows: (1) The complexes in "pdb" format were converted to "gro" format, and the complexes were considered as the initial structures for MD simulations. (2) Preprocessing of aloin was done using AmberTools22 software, with the addition of the Generalized Amber Force Field (GAFF). Hydrogen atoms were added to the small molecules and the Restrained Electrostatic Potential (RESP) was calculated using Gaussian 16W, with the potential data added to the topology file of the MD system. (3) The solvent used was the Three-point transferable intermolecular potential (TIP3P) model, and the complexes were solvated with water molecules, ensuring that the closest distance between protein atoms and the edges of the water box was at least 1.2 nm (12 Å). (4) The system was neutralized by adding an appropriate number of Na^+ and Cl^- ions. Energy minimization (EM) was performed using the steepest descent algorithm to obtain a stable system. And then, it underwent equilibration under both canonical ensemble (NVT) system and constant-pressure, constant-temperature (NPT) system for 100,000 steps, respectively. This coupling constant was set to 0.1 ps, and the duration was 100 ps. (5) MD simulation was performed for the Aloin-protein complexes, consisting of 5,0000,000 steps with a step length of 2 fs and a total duration of 100 ns. (6) The simulation trajectory was saved for subsequent analysis. Based on the MD simulation results, we calculated RMSD, root mean

square fluctuation (RMSF), radius of gyration (Rg), solvent accessible surface area (SASA), and hydrogen bonds (H-bonds) of the complexes. In addition, Gibbs free energy was calculated based on RMSD and Rg values using the "g_sham" and "xpm2txt.py" scripts. In order to investigate the conformational changes of the complexes during the 100 ns simulation, this study used the trajectory of each complex during MD recorded at 20 ns intervals. The 3D conformations of these complexes were derived for comparison.

Experimental Verification in Animal

Establishment and Treatment of Animal Models

The animal model was established using male Sprague-Dawley (SD) rats, aged 6–8 weeks, all obtained from the Lanzhou University Laboratory Animal Center. A total of 30 SD rats were housed in a specific pathogen-free environment, with a 12 h light-dark cycle (7 am to 7 pm as the light phase) and free access to food and water. The rats were randomly divided into five groups (n = 6) as follows: the Normal Control (NC) group, the Experimental Autoimmune Prostatitis (EAP) group, and three EAP groups treated with different doses of Aloin (20, 40, and 80 mg/kg/day), namely Aloin 20 mg/kg, Aloin 40 mg/kg, and Aloin 80 mg/kg groups.

All rats were anesthetized with 2% isoflurane inhalation, and the prostate tissue was surgically exposed. The EAP group and the three Aloin treatment groups received bilateral injections of 50 μL of Complete Freund's Adjuvant (CFA) into each prostate lobe using a sterile syringe. The NC group received an equivalent volume of saline injections.

One week after the injections, the Aloin intervention groups were administered Aloin via gavage at doses of 20, 40, and 80 mg/kg/day. The NC and EAP groups were given equivalent volumes of saline. After a 4-week treatment period, all rats were anesthetized and euthanized using sodium pentobarbital (100 mg/kg). The prostate tissues were promptly excised and weighed to calculate the prostate index, defined as prostate weight (mg) divided by body weight (g) and multiplied by 10. The collected prostate tissues were immediately either frozen at −80 °C or fixed in formaldehyde for future experimental use. Additionally, blood samples were collected from all rats post-euthanasia and processed into serum for subsequent analysis.

Von Frey Filaments in Pain Measurement

The tactile allodynia test was conducted using Von Frey filaments to assess pain behavior at different time points: before modeling (0 weeks), post-modeling (1 week), and after one (2 weeks), two (3 weeks), three (4 weeks), and four weeks (5 weeks) of Aloin treatment (n = 6 per group). Rats were acclimatized in plastic cages for 30 min in a quiet environment before testing. The pain threshold was measured in the perineal area near the scrotum, penis, and prostate using classic Von Frey filaments.

The Von Frey filaments had three different strengths: 2.0 g, 4.0 g, and 6.0 g. Testing began with the 2.0 g filament, applying vertical pressure to the relevant area of the rat's lower abdomen until the filament bent into an S-shape. Each stimulation lasted for 1 to 2s, with intervals of no less than 5s between each application. Each filament strength was tested 50 times, gradually increasing the strength. The interval between adjacent stimuli was set to 1 min, allowing the rats sufficient recovery time between stimuli.

A positive response was defined by the occurrence of any one of the following behaviors: (1) a sudden abdominal contraction, (2) immediate licking or grasping of the stimulation site, or (3) jumping. The response frequency for each group of rats (n = 6) was recorded and statistically analyzed at different time points and filament strengths. Comparisons were made across the groups to assess changes in pain thresholds over time.

Hematoxylin and Eosin (H&E) Staining and Immunohistochemistry (IHC) Staining

Formaldehyde-fixed prostate tissues were dehydrated and embedded in paraffin, and then cut into 4 μm sections for subsequent H&E staining and immunohistochemical staining.

For H&E staining, the slides were deparaffinized first. Then, the slides were treated with the following steps: hematoxylin staining (5 min), water washing (10s), differentiation (HCl/95% alcohol, 1s), water washing (30 min), eosin staining (3 min), and mounting (neutral gum). Then, the sections were observed using microscope (n = 6).

For immunohistochemistry staining of prostate tissue, UltraSensitive^{TM} SP Kits (Fuzhou Maixin Biotech. Co, China) and DAB Kits (Fuzhou Maixin Biotech. Co, China) were used according to the manufacturer's instructions. Sections

were incubated with primary antibodies at 4 °C overnight. Primary antibodies: anti-rabbit Tumor Necrosis Factor-α (TNF-α) antibody (bs-2081R, Bioss, China), anti-rabbit Interleukin-1 beta (IL-1β) antibody (bs-0812R, Bioss, China), anti-rabbit Interleukin-6 (IL-6) antibody (bs-0782R, Bioss, China), anti-rabbit Cyclooxygenase-2 (COX-2) antibody (TA7003, Abmart, China) and anti-rabbit Inducible Nitric Oxide Synthase (iNOS) antibody (TA0199, Abmart, China) (n = 6).

Enzyme-Linked Immunosorbent Assay (ELISA)

Blood samples from rats were collected from the heart, left at room temperature for 0.5 h, and then centrifuged at 3000 rpm for 15 min at 4°C. After centrifugation, serum was taken to detect the inflammatory factors TNF-α, IL-6, and IL-1β by ELISA (Ruixinbio, Quanzhou, China). The specific procedures are referred to ELISA kit instructions (n = 6).

Detection of Oxidative Stress Level

The oxidative stress levels of rat prostate tissues were determined by Catalase (CAT) Assay Kit (Abbkine Scientific Co., Ltd, Wuhan, China), Superoxide Dismutase (SOD) Assay Kit (Abbkine Scientific Co., Ltd, Wuhan, China) and Malondialdehyde (MDA) Assay Kit (Abbkine Scientific Co., Ltd, Wuhan, China). The levels of CAT, SOD, and MDA in prostate tissues were measured by following the manufacturer's instructions (Abbkine Scientific Co., Ltd, Wuhan, China) (n = 6).

Quantitative Real-Time Polymerase Chain Reaction (qRT-PCR)

Prostate tissue was thoroughly ground in liquid nitrogen and subsequently homogenized in Trizol reagent (Accurate Biotechnology Co., Ltd, Changsha, China), followed by Ribonucleic Acid (RNA) extraction according to the manufacturer's protocol. 5× Evo M-MLV RT Reaction Mix Ver.2 (Accurate Biotechnology Co., Ltd, Changsha, China) is used for RNA reverse transcription according to the manufacturer's instructions. Complementary Deoxyribonucleic Acid (cDNA) was generated by reverse transcription for subsequent qRT-PCR.

The qRT-PCR reaction system consisted of 10 μL 2× SYBR Green Pro Taq HS Premix (Accurate Biotechnology Co., Ltd, Changsha, China), 0.4 μL of each upstream and downstream primer (10 μM), 2 μL cDNA template, and 7.2 μL RNase-free water. Real-time fluorescent quantitative PCR was performed using the CFX96 real-time PCR detection system (Bio-Rad, Hercules, CA, USA). qRT-PCR reaction condition was set as follows: holding stage 95 °C for 120s, cycling stage 95 °C for 3s, 60 °C for 30s, with total cycles of 40, and melting curve stage at 95 °C for 5s, 65 °C to 95 °C with a temperature increment of 0.5 °C and 5s to plate read for each temperature. All data were normalized to β-actin expression and $2^{-\Delta\Delta Ct}$ method was applied to analyze Messenger Ribonucleic Acid (mRNA) expression (n = 6).

The primers were listed as follows:

IL-6 (Rat): Forward: 5′-CCAGTTGCCTTCTTGGGACT-3′,
Reverse: 5′-TGCCATTGCACAACTCTTTTC-3′.
IL-1β (Rat): Forward: 5′-AGGAGAGACAAGCAACGACA-3′,
Reverse: 5′-TTGTTTGGGATCCACACTCTCC-3′.
TNF-α (Rat): Forward: 5′-TGGGCTCCCTCTCATCAGTT-3′,
Reverse: 5′-TCCGCTTGGTGGTTTGCTAC-3′.
β-actin (Rat): Forward: 5′-ACCCGCGAGTACAACCTTCT-3′,
Reverse: 5′-GCCGTGTTCAATGGGGTACT-3′.
AKT1 (Rat): Forward: 5′- GAGACGATGGACTTCCGGTC-3′,
Reverse: 5′-ACTCGTTCATGGTCACACGG-3′.
EGFR (Rat): Forward: 5′- TCAACAACCAGAAGGGCCAAA-3′,
Reverse: 5′-CATGAAGAGGCCGATCCCAA-3′.
ESR1 (Rat): Forward: 5′-TTTTGAACCAGCAGGGTGGC-3′,
Reverse: 5′-TGTTGTCCACGTACACCTCG-3′.
HSP90AA1 (Rat): Forward: 5′-GCAGCAAAGAAACACCTGGAG-3′,
Reverse: 5′-TCATCCTCATCAATACCTAGACCA-3′.
SRC (Rat): Forward: 5′-AAACACTCAGGTCAAGGCTGAT-3′,

Reverse: 5′-GCCTCTGTATTCTGTCCTGAGCTA-3′.

Statistical Analysis

All data are expressed as the mean ± SD. GraphPad Prism 9.5.0 software was utilized to conduct statistical analyses and generate graphs. First, Q-Q plots were performed to assess the normality of the data. If the data showed normality, the significance of the difference between multiple groups was analyzed by one-way ANOVA followed by Tukey's post hoc test. For non-normally distributed data or data with heteroscedasticity, the Kruskal–Wallis test or Welch's ANOVA was used to assess statistical significance. A p-value less than 0.05 was considered statistically significant (*$p < 0.05$, **$p < 0.01$, ***$p < 0.001$, ****$p < 0.0001$).

Results

Prediction of Targets and Construction of PPI Networks

To obtain the potential Aloin targets, four databases were searched: 36 genes from the SwissTargetPrediction database, 106 genes from the Superpred database, 4 genes from the TCMSP database, and 304 genes from the PharmMapper database were combined to yield a total of 409 drug targets. The search terms "chronic prostatitis with chronic pelvic pain syndrome" were entered into GeneCards, OMIM, and DisGENET to obtain related genes of CP/CPPS. The search results revealed 3791 genes in GeneCards, 556 in OMIM, and 8 genes in DisGENET. After combining and deduplicating, 4284 CP/CPPS targets were obtained. A total of 235 potential targets relevant to Aloin for the treatment of chronic prostatitis were identified by integrating drug and disease targets (Figure 2A and B). To delve deeper into the mechanisms underlying Aloin's therapeutic potential in CP/CPPS, the 235 shared targets were employed to build PPI network, which exhibited 110 nodes and 1358 edges (Figure 2C).

GO and KEGG Pathway Enrichment Analysis

The GO results for the common targets of Aloin and CP/CPPS showed a total of 2916 enrichment results. Of these, 2562 were related to BP, 94 to CC, and 260 to MF. The top 10 ranked GO terms for BP, CC, and MF were selected for visualization (Figure 3A–D). These results suggest that Aloin may be essential in treating CP/CPPS via multiple functions.

KEGG pathway analysis for the common targets of Aloin and CP/CPPS yielded a total of 172 pathways, and the top 10 pathways were selected for mapping (Figure 3E).

To better highlight the GO terms and KEGG pathways potentially associated with CP/CPPS, the GO terms (Figure 3F) and KEGG pathways (Figure 3G) related to immune responses, oxidative stress, and the involvement of core targets were presented separately.

Molecular Docking Validation

Based on the previous analysis, AKT1, EGFR, HSP90AA1, SRC, and ESR1 were selected as core targets for molecular docking to verify their interaction activities with Aloin. The binding affinity was used to indicate the strength of Aloin's interaction with the target proteins.

The docking results indicate that Aloin can access the active sites of the target proteins, and the interactions of Aloin with the top five core targets were selected for visualization. Specifically, Aloin forms a hydrogen bond with Thr160 of AKT1 (Figure 4A). For EGFR, Aloin forms hydrogen bonds with Arg817, Asn818, Asp831, Ser696, Leu694, and Met769 (Figure 4B). Regarding ESR1, hydrogen bonds are formed with Ser456, Asn455, Arg515, and Ser512 (Figure 4C). Aloin also forms hydrogen bonds with Tyr139, Asn51, Asp54, and Gly97 of HSP90AA1 (Figure 4D). Additionally, with SRC, hydrogen bonds are formed with Val137, Ser134, Asn135, Tyr90, and Glu147 (Figure 4E). The binding free energies of AKT1, EGFR, HSP90AA1, SRC, and ESR1 with Aloin were −7.2, −7.6, −7.9, −8.4, and −7.9 kcal/mol, respectively (Table 1). These results indicate that Aloin exhibits a strong binding affinity for the target proteins.

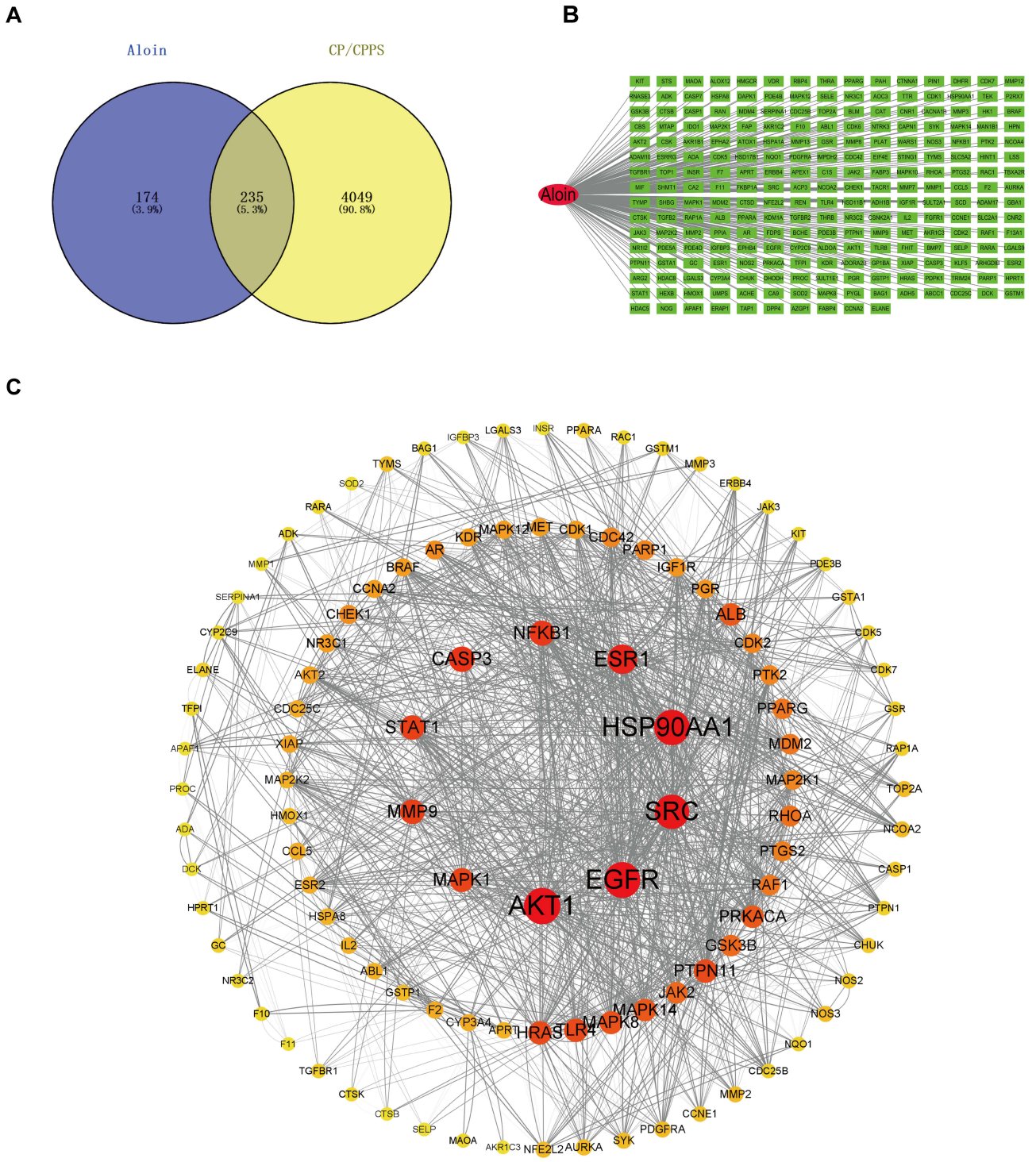

Figure 2 The network pharmacology analysis of aloin in the treatment of CP/CPPS. (**A**) Aloin and CP/CPPS common targets. (**B**) Drug-target prediction results.(**C**) The PPI network of Aloin targets against CP/CPPS constructed by Cytoscape.

Molecular Dynamics Simulation

To further investigate the molecular docking results, GROMACS 2022.03 software was utilized to perform 100 ns molecular dynamics simulations on the complexes formed by Aloin with AKT1, EGFR, ESR1, HSP90AA1, and SRC. The stability of these complexes was assessed using RMSD, RMSF, Rg, hydrogen bond analysis, and SASA. Additionally, GROMACS scripts "g_sham" and "xpm2txt.py" were employed to calculate Gibbs free energy based on

https://doi.org/10.2147/DDDT.S473678

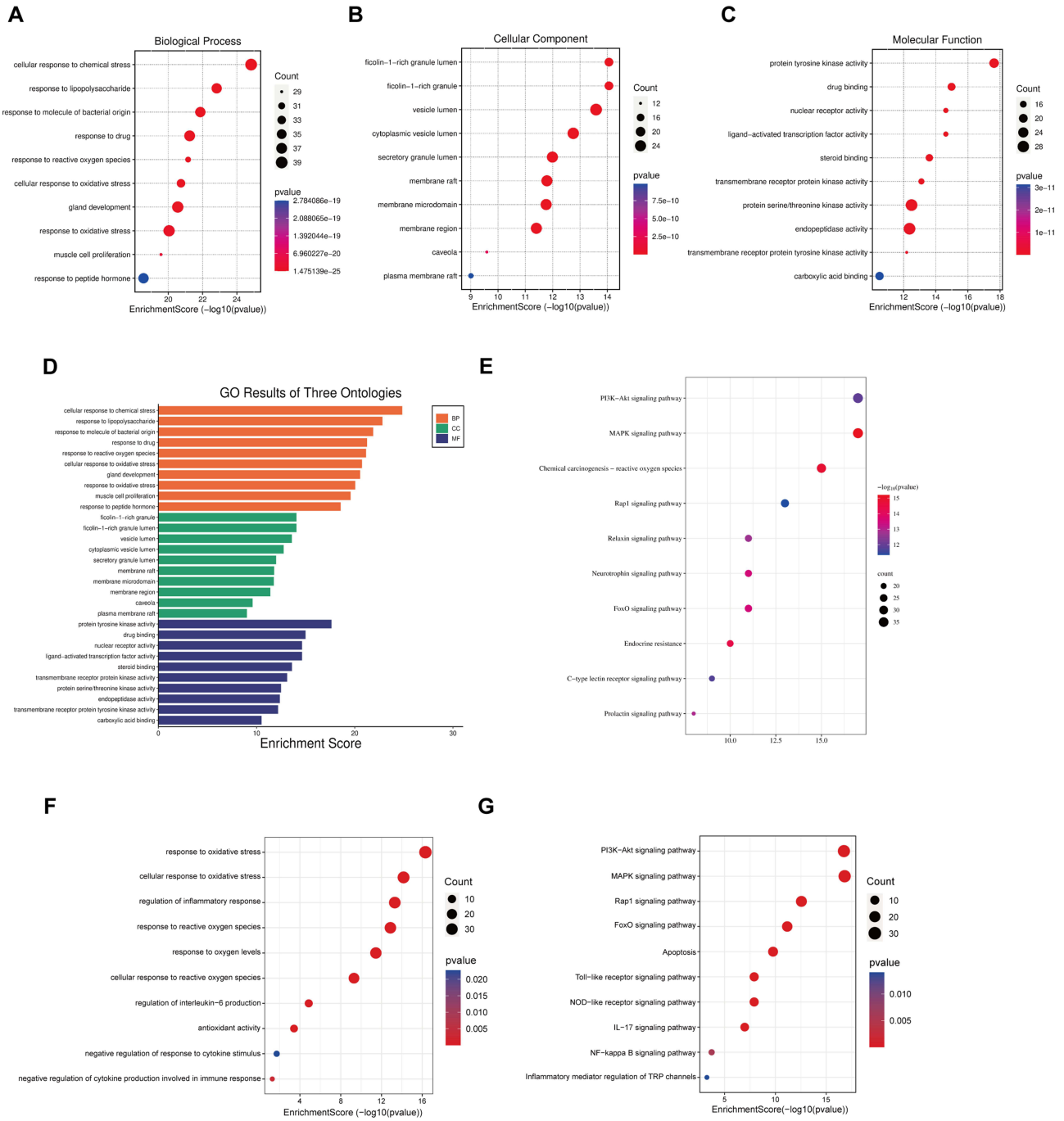

Figure 3 Analysis of GO and KEGG enrichment for target intersection. (**A-C**) GO enrichment analysis of aloin and CP/CPPS common targets. (**D**) GO enrichment results of BP, MF, and CC. (**E**) KEGG enrichment analysis of aloin and CP/CPPS common targets. (**F**) GO terms related to immune responses, oxidative stress, and the involvement of core targets. (**G**) KEGG pathways related to immune responses, oxidative stress, and the involvement of core targets.

the RMSD and Rg values of the complexes. Snapshots of the complexes were taken at 0 ns, 20 ns, 40 ns, 60 ns, 80 ns, and 100 ns to observe structural changes during the simulations.

RMSD analysis reveals the positional differences between the conformations generated by the protein simulations and their initial conformations. Compared to the RMSD curves of the free proteins, the RMSD curves for the Aloin-AKT1, Aloin-EGFR, and Aloin-ESR1 complexes reached equilibrium after 40 ns, with mean RMSD values of 0.25 nm, 0.27 nm, and 0.32 nm, respectively (Figure 5A–C). In contrast, the RMSD curves for the Aloin-HSP90AA1 and Aloin-SRC complexes exhibited fluctuations throughout the simulation, with mean RMSD values of 0.21 nm and 0.29 nm

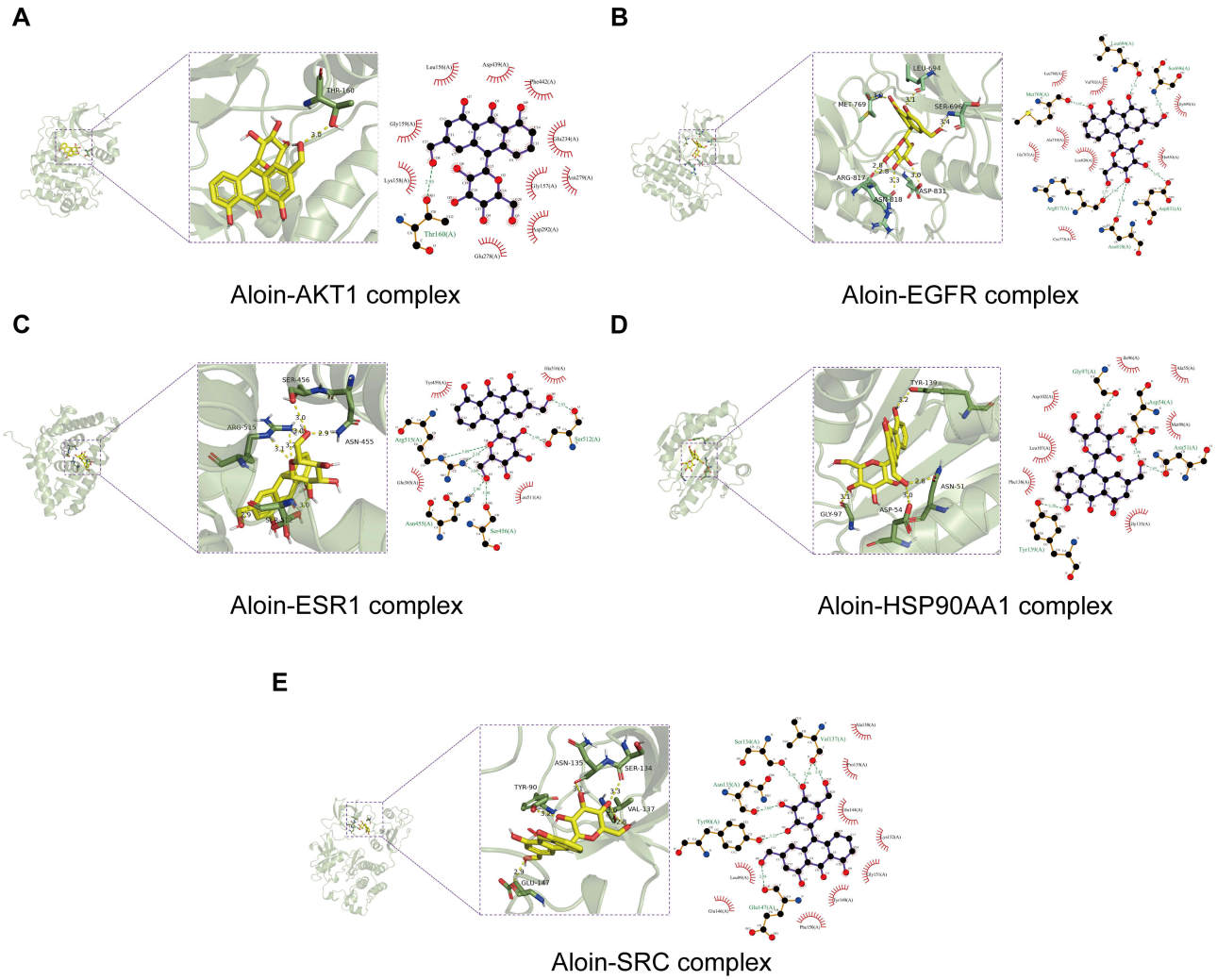

Figure 4 Molecular docking patterns of Aloin and core targets. Aloin docked with: (**A**) AKT1, (**B**) EGFR, (**C**) ESR1, (**D**) HSP90AA1, and (**E**) SRC.

(Figure 5D–E). These results suggest that AKT1, EGFR, and ESR1 demonstrate improved stability upon binding to Aloin compared to their free counterparts.

RMSF analysis provides insight into the flexibility and movement of protein amino acids. The results show that, upon binding, the RMSF curves for the Aloin-AKT1 (Figure 6A), Aloin-EGFR (Figure 6B), Aloin-ESR1 (Figure 6C), and Aloin-HSP90AA1 (Figure 6D) complexes were significantly reduced compared to the free proteins. However, the RMSF curve for the Aloin-SRC complex (Figure 6E) did not show significant differences from that of the free proteins,

Table 1 Docking Results of Aloin With Core Target Proteins

Target	PDB ID	Compound	Binding Energy (kcal/mol)
AKT1	6NPZ	Aloin	−7.2
EGFR	2GS2		−7.6
HSP90AA1	6U98		−7.9
SRC	2SRC		−8.4
ESR1	6SBO		−7.9

https://doi.org/10.2147/DDDT.S473678

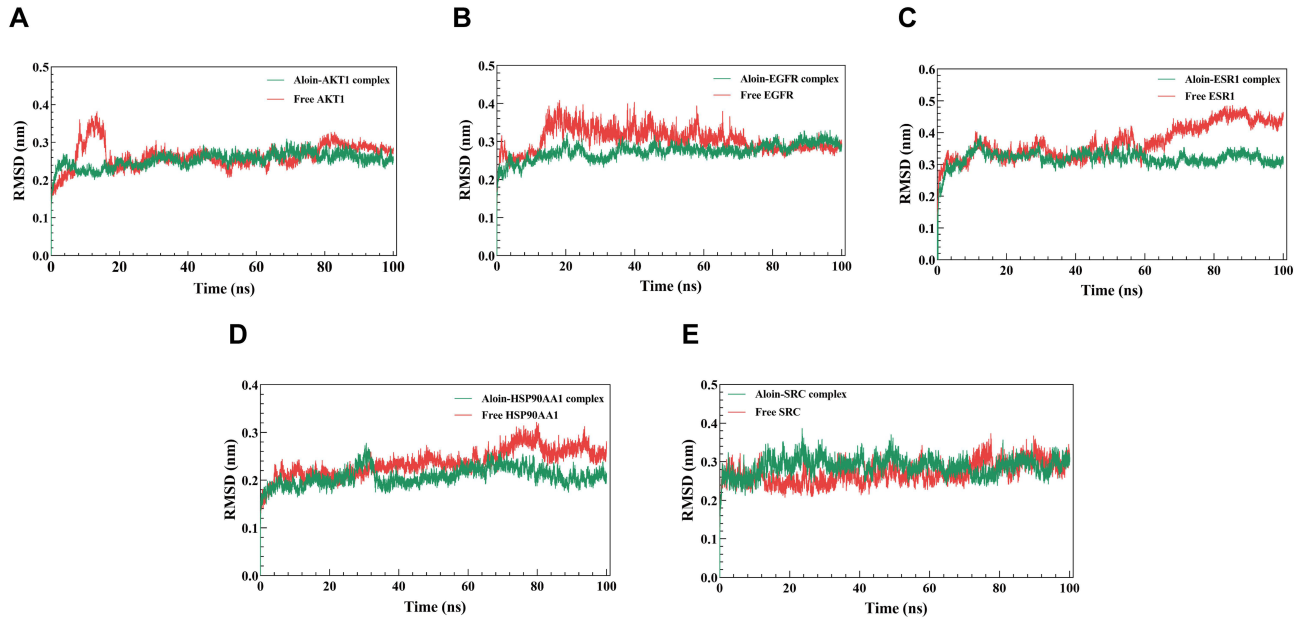

Figure 5 RMSD analysis of protein-small molecule complexes during 100 ns simulation. (**A**) RMSD curves of Aloin-AKT1 complex. (**B**) RMSD curves of Aloin-EGFR complex. (**C**) RMSD curves of Aloin-ESR1 complex. (**D**) RMSD curves of Aloin-HSP90AA1 complex. (**E**) RMSD curves of Aloin-SRC complex. The red lines represent the RMSD curve of the free proteins, and the green lines represent the RMSD curve of the complexes.

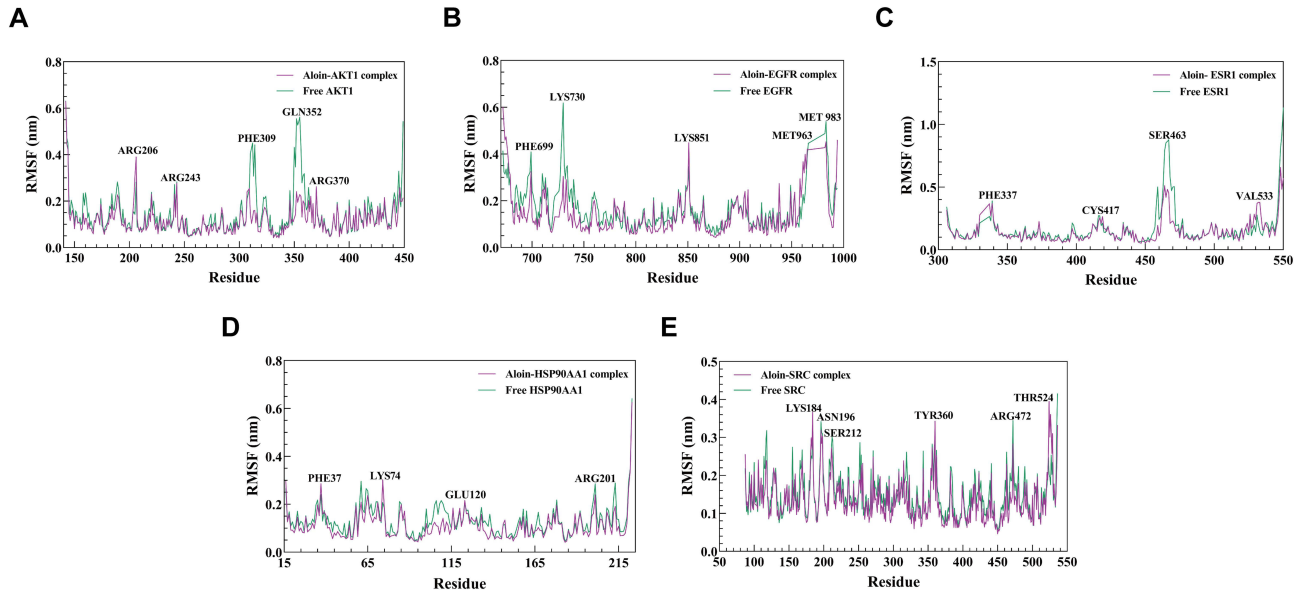

Figure 6 RMSF analysis of protein-small molecule complexes during 100 ns simulation. (**A**) RMSF curves of Aloin-AKT1 complex. (**B**) RMSF curves of Aloin-EGFR complex. (**C**) RMSF curves of Aloin-ESR1 complex. (**D**) RMSF curves of Aloin-HSP90AA1 complex. (**E**) RMSF curves of Aloin-SRC complex. The green lines represent the RMSF curve of the free proteins, and the purple lines represent the RMSF curve of the complexes.

indicating that binding of Aloin significantly reduces the amino acid flexibility of AKT1, EGFR, ESR1, and HSP90AA1. Therefore, Aloin appears to enhance the stability and enzymatic activity of these proteins.

Rg is a measure of the compactness of a protein's structure, where a more stable protein corresponds to smaller Rg values. The Rg curves for the Aloin-AKT1 (Figure 7A), Aloin-EGFR (Figure 7B), Aloin-ESR1 (Figure 7C), and Aloin-HSP90AA1 (Figure 7D) complexes remained relatively stable throughout the 100 ns simulation compared to the free proteins. Additionally, the Rg values for these complexes were consistently lower than those of the free proteins, whereas

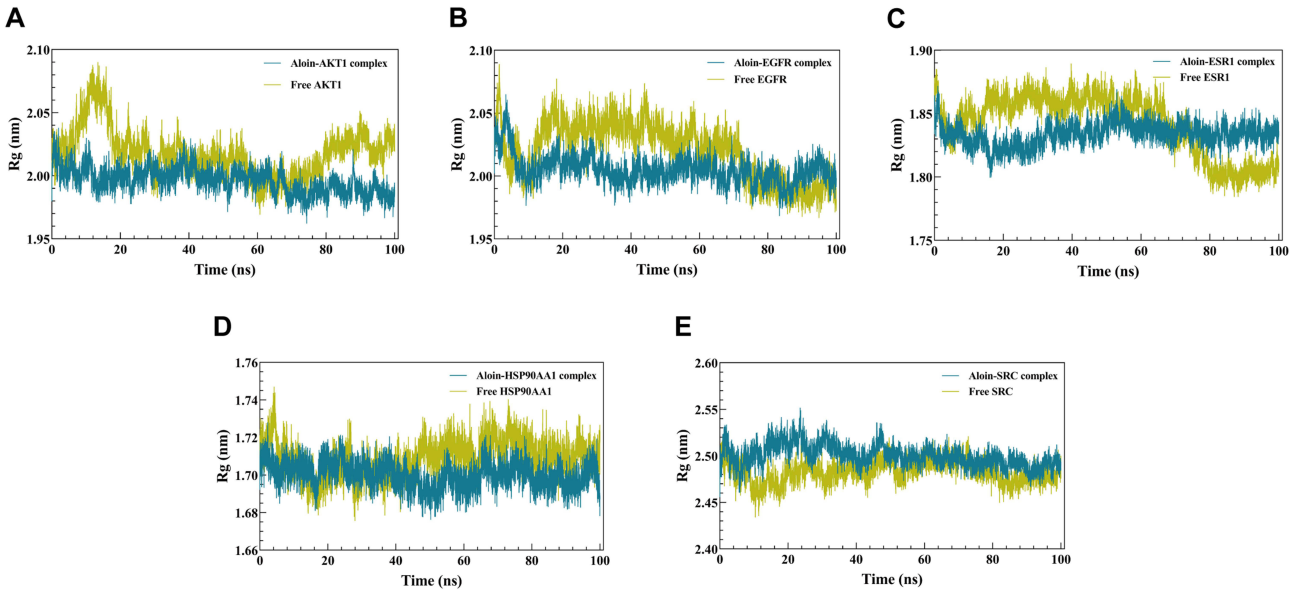

Figure 7 Rg analysis of protein-small molecule complexes during 100 ns simulations. (**A**) Rg curves of Aloin-AKT1 complex. (**B**) Rg curves of Aloin-EGFR complex. (**C**) Rg curves of Aloin-ESR1 complex. (**D**) Rg curves of Aloin-HSP90AA1 complex. (**E**) Rg curves of Aloin-SRC complex. The yellow lines represent the Rg curve of the free proteins, and the blue lines represent the Rg curve of the complexes.

the Rg of the Aloin-SRC complex (Figure 7E) showed no significant difference, suggesting that Aloin binds more firmly to AKT1, EGFR, ESR1, and HSP90AA1.

Hydrogen bonds are among the strongest non-covalent interactions, making it crucial to understand the binding affinity between a ligand and a protein. The number of hydrogen bonds in the Aloin-AKT1 (Figure 8A), Aloin-EGFR (Figure 8B), Aloin-ESR1 (Figure 8C), Aloin-HSP90AA1 (Figure 8D), and Aloin-SRC (Figure 8E) complexes ranged from 0–8, 0–7, 0–5, 0–7, and 0–7, respectively. This indicates that the number of hydrogen bonds formed in all complexes remained relatively constant throughout the simulation process.

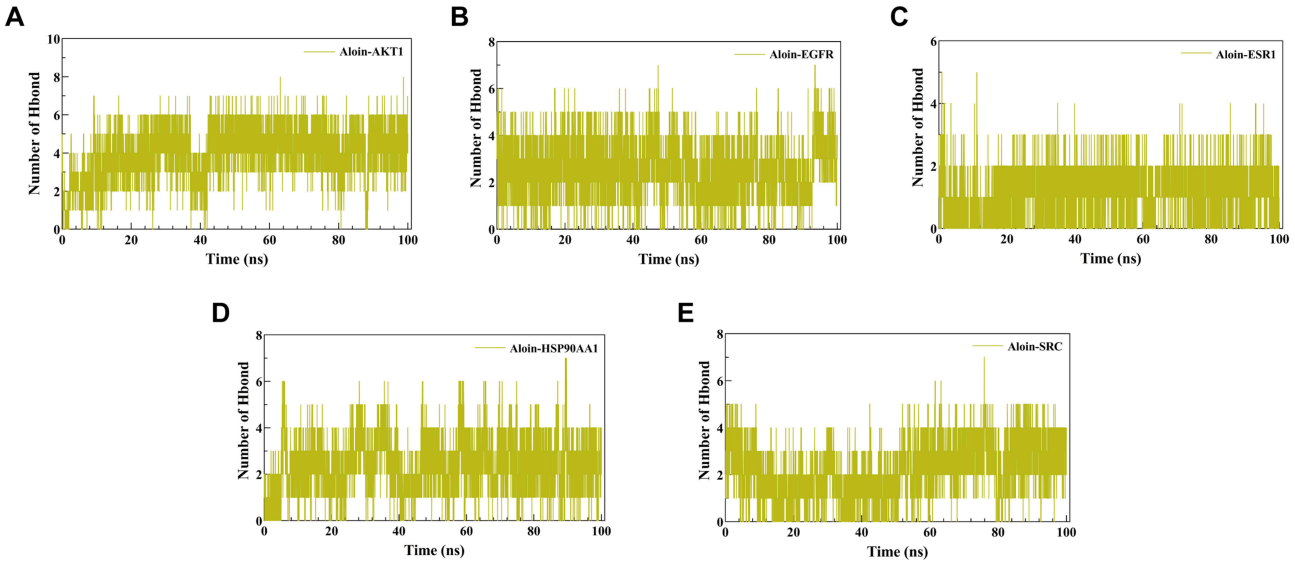

Figure 8 Hydrogen bonding analysis of protein-small molecule complexes during 100 ns simulations. (**A**) Hydrogen bonding analysis of Aloin-AKT1 complex. (**B**) Hydrogen bonding analysis of Aloin-EGFR complex. (**C**) Hydrogen bonding analysis of Aloin-ESR1 complex. (**D**) Hydrogen bonding analysis of Aloin-HSP90AA1 complex. (**E**) Hydrogen bonding analysis of Aloin-SRC complex.

https://doi.org/10.2147/DDDT.S473678

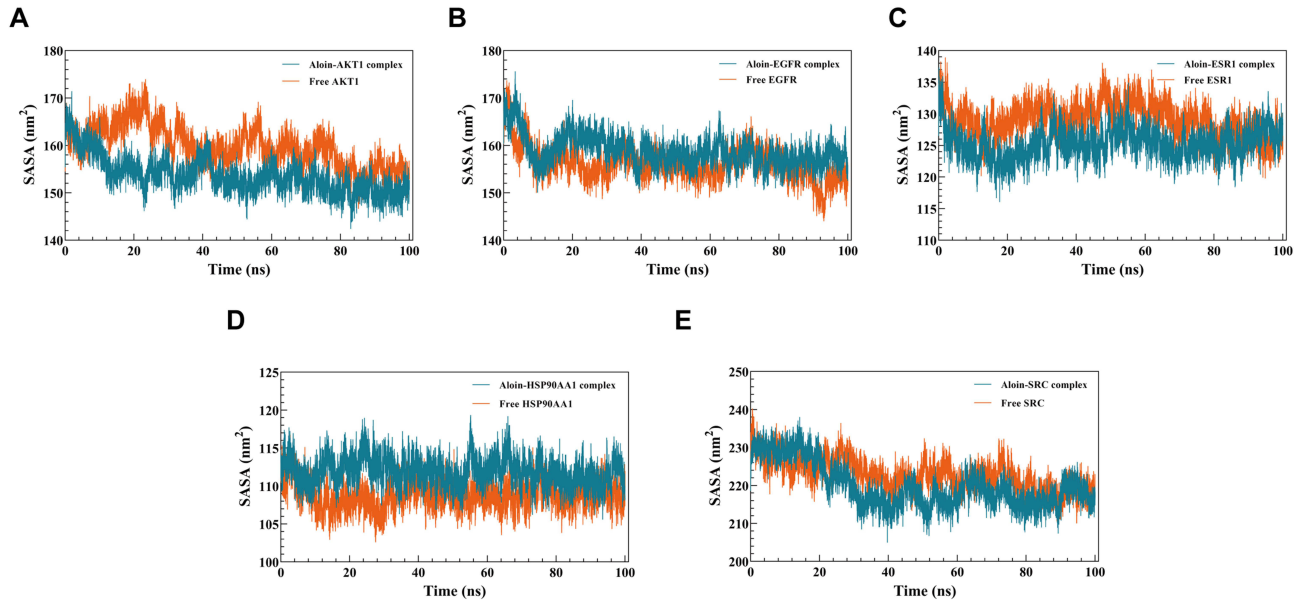

Figure 9 SASA analysis of protein-small molecule complexes during 100 ns simulations. (**A**) SASA curves of Aloin-AKT1 complex. (**B**) SASA curves of Aloin-EGFR complex. (**C**) SASA curves of Aloin-ESR1 complex. (**D**) SASA curves of Aloin-HSP90AA1 complex. (**E**) SASA curves of Aloin-SRC complex. The Orange lines represent the SASA curve of the free proteins, while the blue lines represent the SASA curve of the complexes.

SASA represents the surface area of a macromolecule exposed to the solution. This value is influenced by the hydrophilicity of the macromolecule, with residues of higher surface energy generally exhibiting larger SASA values. A smaller SASA value indicates a tighter protein fold and less susceptibility to thermal denaturation. The SASA curves for the Aloin-AKT1 complex (Figure 9A) showed a significant reduction compared to the free protein, while no significant effect was observed for EGFR (Figure 9B). The SASA curves for the Aloin-ESR1 (Figure 9C) were significantly reduced compared to the free protein. But the SASA curves for Aloin-HSP90AA1 (Figure 9D) complexes, compared with those of the free protein, showed a slight increase, whereas no significant difference was found for Aloin-SRC (Figure 9E) compared to the free protein. This suggests potential hydrophobic interactions between Aloin and AKT1, ESR1 that may contribute to a more compact complex.

Gibbs free energy landscape 3D plots were generated using the RMSD, Rg, and Gibbs free energy values of the complexes. These maps provide insights into the stability of the complexes, with regions shaded in blue and darker blue indicating lower energy states achievable at steady-state conformations. In contrast, weak or unstable protein-ligand interactions yield multiple, surface-rough minimum energy clusters, while strong interactions are represented by nearly single and smooth energy clusters in the potential energy distribution. Compared to the Gibbs free energy 3D landscape maps of free proteins, those for the Aloin-AKT1 (Figure 10A), Aloin-EGFR (Figure 10B), Aloin-ESR1 (Figure 10C), and Aloin-HSP90AA1 (Figure 10D) complexes exhibit single, sharp minimum energy clusters. The Gibbs free energy 3D profile for the Aloin-SRC complex (Figure 10E) shows no significant difference from that of free SRC, indicating that Aloin can form stable complex systems with AKT1, EGFR, ESR1, and HSP90AA1.

To investigate the conformational changes in the Aloin-AKT1, Aloin-EGFR, Aloin-ESR1, Aloin-HSP90AA1, and Aloin-SRC complexes during the 100 ns simulation, motion trajectories recorded at 20 ns intervals were analyzed. The trajectory snapshots of the Aloin-AKT1 (Figure S2), Aloin-EGFR (Figure S3), Aloin-ESR1 (Figure S4), and Aloin-HSP90AA1 complexes (Figure S5) over the 100 ns period revealed minimal shifts in the position of Aloin within the active pockets of AKT1, EGFR, ESR1, and HSP90AA1, indicating stable binding following a slight initial deflection from the starting conformation at 0 ns. Conversely, the docking of Aloin with SRC resulted in significant displacement and deviation from the initial conformation (0 ns) at the stabilization point (after 40 ns) (Figure S6).

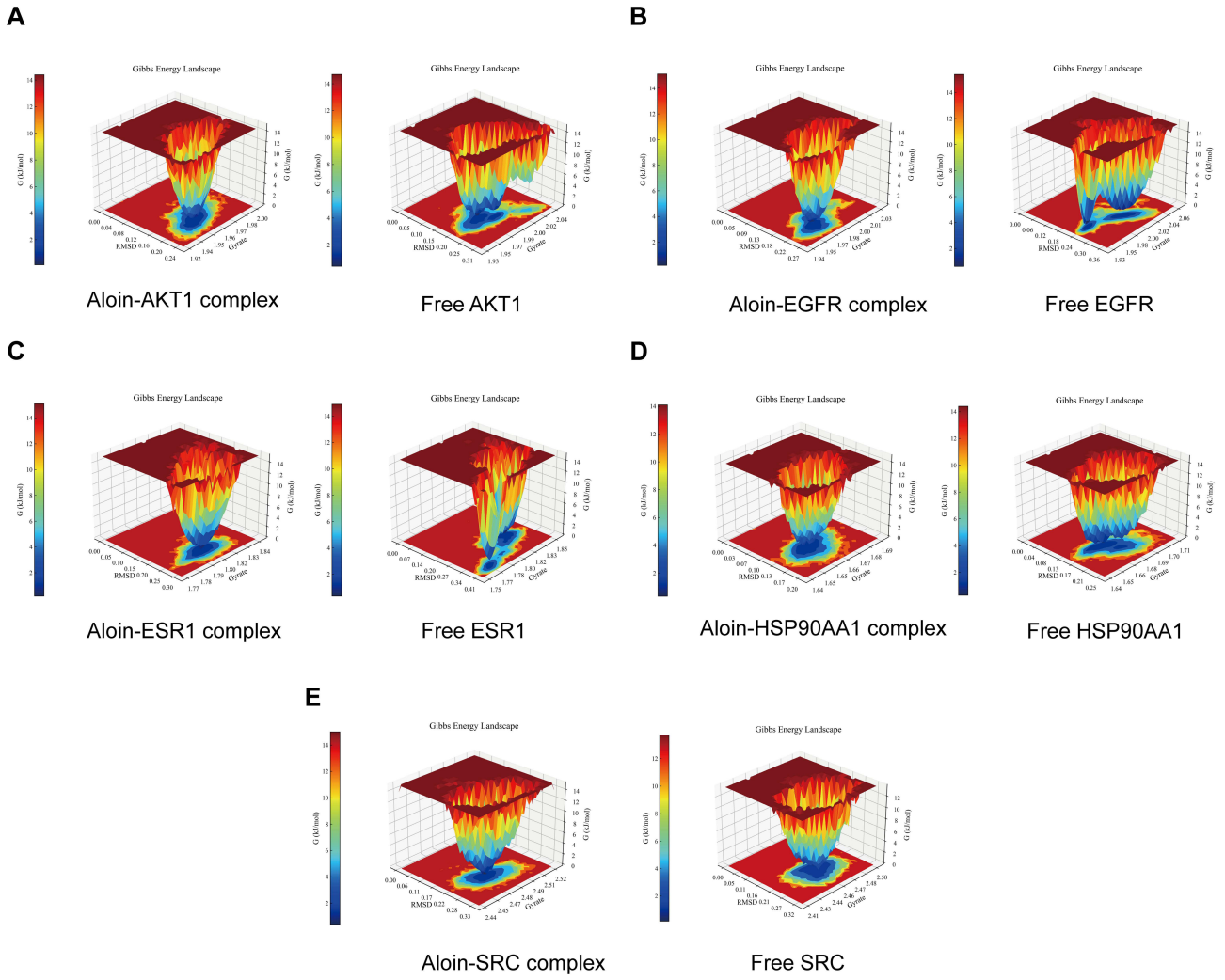

Figure 10 Gibbs free energy analysis of protein-small molecule complexes and free proteins. (**A**) Gibbs free energy 3D morphology of Aloin-AKT1 complex and free AKT1. (**B**) Gibbs free energy 3D morphology of Aloin-EGFR complex and free EGFR. (**C**) Gibbs free energy 3D morphology of Aloin-ESR1 complex and free HSP90AA1. (**D**) Gibbs free energy 3D morphology of Aloin-HSP90AA1 complex and free ESR1. (**E**) Gibbs free energy 3D morphology of Aloin-SRC complex and free SRC.

Aloin Inhibits the Decrease of Pain Threshold and Hypersensitivity in the Pelvic Area in CP/CPPS Model Rats

To explore the role of Aloin in treating CP/CPPS, we established the animal model of chronic prostatitis through intraprostatic injection of CFA and administered various doses (20 mg/kg, 40 mg/kg, 80 mg/kg) of Aloin to observe pain threshold changes in the model animals. We assessed the pain sensitivity of rats using Von Frey filaments of three different strengths: 2.0 g, 4.0 g, and 6.0 g. The results of the 2.0 g filament pain test (Figure 11A) showed that there were no significant differences in the response frequency among the groups prior to modeling (0 weeks) (NC: 2.67 ± 1.37, EAP: 3.17 ± 0.75, Aloin 20 mg/kg: 2.50 ± 0.84, Aloin 40 mg/kg: 2.67 ± 0.82, Aloin 80 mg/kg: 2.00 ± 0.63, $p > 0.05$ for all comparisons with the NC group, $n = 6$). In the first assessment after model establishment (1 week), the response frequency in the EAP group and the Aloin 20 mg/kg, Aloin 40 mg/kg, and Aloin 80 mg/kg groups significantly increased compared to the NC group (NC: 3.50 ± 1.38, EAP: 20.50 ± 1.87, Aloin 20 mg/kg: 20.00 ± 0.89, Aloin 40 mg/kg: 20.00 ± 1.10, Aloin 80 mg/kg: 19.17 ± 0.98, $p < 0.0001$, $n = 6$), indicating that the pain threshold was reduced in the prostatitis model compared to normal animals. After 4 weeks of Aloin treatment (5 weeks), the response frequency in the EAP model group remained significantly higher than in the NC group (NC: 2.167 ± 0.98, EAP: 18.50 ± 0.84, $p < 0.0001$ for comparison with the NC group, $n = 6$). However, the response frequency in the Aloin 20 mg/kg, Aloin 40 mg/kg, and

https://doi.org/10.2147/DDDT.S473678

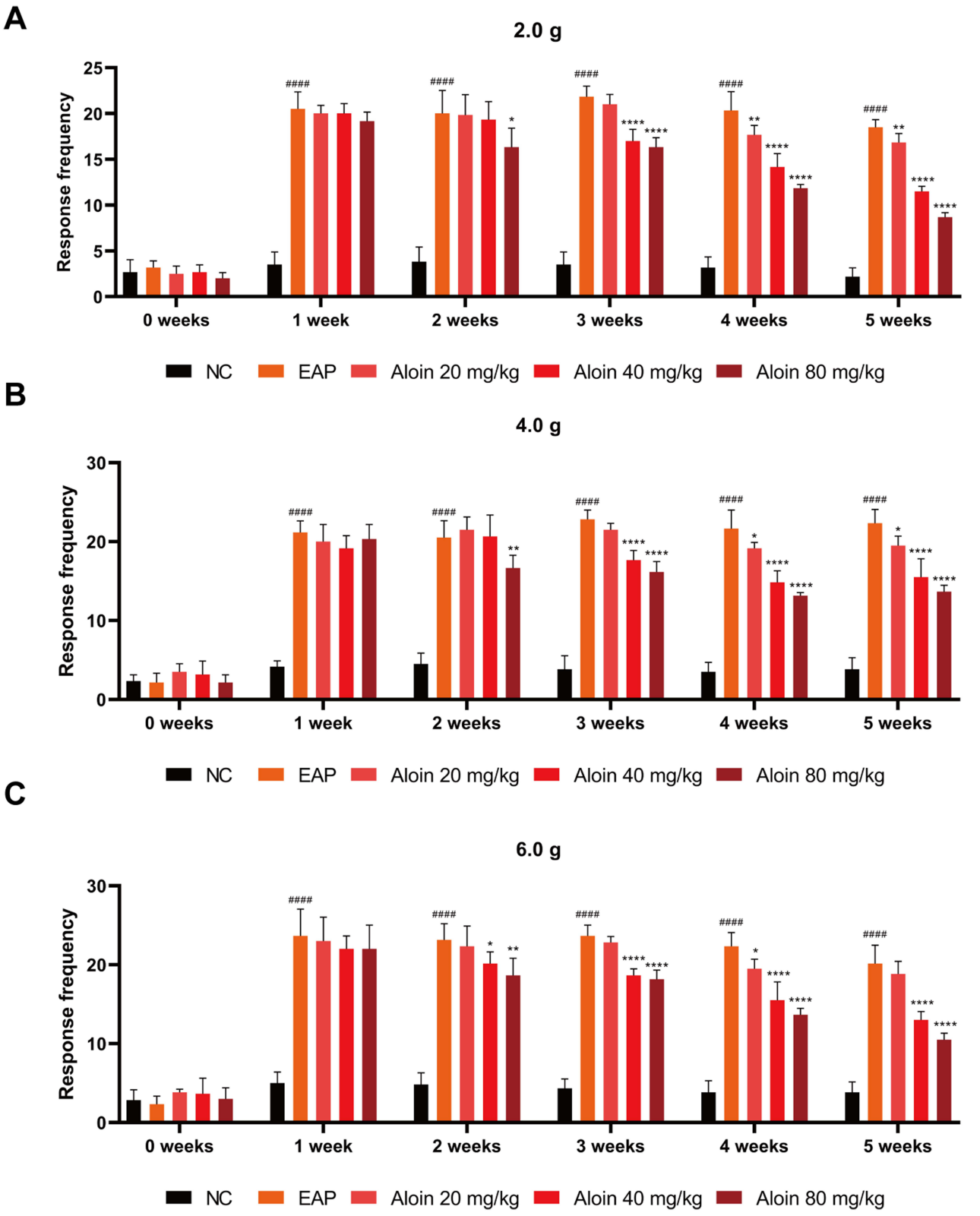

Figure 11 The frequencies of pelvic pain positive responses of rats in different groups were assessed by the Von Frey test. (**A**) Von Frey filament strength: 2.0 g (n = 6). (**B**) Von Frey filament strength: 4.0 g (n = 6). (**C**) Von Frey filament strength: 6.0 g (n = 6). Data are presented as mean ± SD. The symbol "#" indicates a comparison between the EAP group and the NC group; the symbol "*" indicates a comparison between the EAP group and the Aloin intervention groups. Significance is denoted as $^{\#\#\#\#}p < 0.0001$ vs NC group and $^{*}p < 0.05$, $^{**}p < 0.01$, $^{****}p < 0.0001$ vs EAP group.

Aloin 80 mg/kg groups was significantly lower than in the EAP group (Aloin 20 mg/kg: 16.83 ± 0.98, p< 0.01, n = 6; Aloin 40 mg/kg: 11.50 ± 0.55, p< 0.0001, n = 6; Aloin 80 mg/kg: 8.67 ± 0.52, p< 0.0001, n = 6), suggesting that Aloin alleviated pain symptoms in CP/CPPS rats. Similar results were observed in the 4.0 g filament test (Figure 11B) and the 6.0 g filament test (Figure 11C). The detailed response frequencies and p-values are provided in Table S1 (2.0 g), Table S2 (4.0 g), and Table S3 (6.0 g). These findings suggest that Aloin effectively improves the reduced pain threshold in CP/CPPS rats.

Aloin Reduces Inflammatory Infiltration and Inflammatory Factor Levels in Animal Models

Gross morphological examination revealed that rats in the EAP group exhibited a marked increase in prostate volume, with more pronounced tissue congestion and edema compared to the NC group (Figure 12A). Histopathological analysis using H&E staining demonstrated a significant increase in inflammatory cell infiltration within the prostatic interstitium in the EAP group relative to the NC group (Figure 12B). However, Aloin treatment significantly reduced the extent of inflammatory cell infiltration in the prostate tissue.

At the end of the experiment, body weights of all rats were recorded, with no significant differences observed across the groups (Figure 12C). The body weights were as follows: NC: 367.2 ± 31.68 g, EAP: 372.6 ± 28.96 g, Aloin 20 mg/kg: 372.2 ± 31.27 g, Aloin 40 mg/kg: 365.8 ± 53.56 g, Aloin 80 mg/kg: 383.2 ± 28.96 g ($p > 0.05$ for all comparisons with the NC group, n = 6). Prostate weights were also measured, and the prostate index was calculated (Figure 12D). While the prostate indices in the Aloin 20 mg/kg and 40 mg/kg groups were lower than in the EAP group (EAP: 19.40 ± 3.48, n = 6; NC: 12.81 ± 1.64, $p < 0.001$ for comparison with EAP group, n = 6), the differences were not statistically significant (Aloin 20 mg/kg: 16.42 ± 3.21, p = 0.19, n = 6; Aloin 40 mg/kg: 15.88 ± 2.93, p = 0.10, n = 6). However, treatment with 80 mg/kg of Aloin significantly reduced the prostate index (Aloin 80 mg/kg: 13.33 ± 1.39; $p < 0.01$, n = 6).

IHC staining revealed elevated levels of inflammatory markers in the prostates of the EAP group, which were significantly reduced following Aloin treatment. In particular, Aloin reduced the expression of key inflammatory cytokines such as IL-6, TNF-α, and IL-1β (Figure 13A). RT-qPCR results corroborated these findings. IL-1β expression was significantly higher in the EAP group than in the NC group (NC: 1.000 ± 0.096, n = 6, EAP: 2.121 ± 0.195; $p < 0.0001$, n = 6). Aloin treatment at doses of 20, 40, and 80 mg/kg significantly reduced IL-1β expression compared to the EAP group (Aloin 20 mg/kg: 1.831 ± 0.211, $p < 0.05$, n = 6; Aloin 40 mg/kg: 1.229 ± 0.060, $p < 0.0001$, n = 6; Aloin 80 mg/kg: 1.144 ± 0.093, $p < 0.0001$, n = 6) (Figure 13B). Similarly, IL-6 expression was markedly elevated in the EAP group compared to the NC group (NC: 1.000 ± 0.245, n = 6, EAP: 3.885 ± 0.500, $p < 0.0001$, n = 6), but significantly decreased following Aloin intervention (Aloin 20 mg/kg: 2.762 ± 0.564, $p < 0.001$, n = 6; Aloin 40 mg/kg: 2.025 ± 0.166, $p < 0.0001$, n = 6; Aloin 80 mg/kg: 1.301 ± 0.174, $p < 0.0001$, n = 6) (Figure 13C). Furthermore, TNF-α expression was significantly elevated in the EAP group compared to the NC group (NC: 1.000 ± 0.179, n = 6, EAP: 2.959 ± 0.536, $p < 0.0001$, n = 6). Treatment with Aloin at 40 mg/kg and 80 mg/kg significantly reduced TNF-α expression (Aloin 20 mg/kg: 2.680 ± 0.769, $p > 0.05$, n = 6; Aloin 40 mg/kg: 1.661 ± 0.536, $p < 0.01$, n = 6; Aloin 80 mg/kg: 1.315 ± 0.331, $p < 0.0001$, n = 6) (Figure 13D).

ELISA were performed to quantify the serum levels of inflammatory markers IL-1β, IL-6, and TNF-α in rats, further supporting these findings. IL-1β levels in the EAP group were significantly higher than those in the NC group (NC: 17.68 ± 1.92 pg/mL, EAP: 37.76 ± 2.61 pg/mL, $p < 0.0001$, n = 6), while Aloin treatment at doses of 40 mg/kg (27.27 ± 2.48 pg/mL, $p < 0.0001$, n = 6) and 80 mg/kg (22.30 ± 3.53 pg/mL, $p < 0.0001$, n = 6) significantly reduced IL-1β levels compared to the EAP group, although the 20 mg/kg dose did not achieve statistical significance (34.36 ± 3.95 pg/mL, p = 0.3092, n = 6) (Figure 13E). As shown in Figure 13F, serum IL-6 levels were significantly higher in the EAP group compared to the NC group (NC: 53.05 ± 10.54 pg/mL, EAP: 132.6 ± 8.91 pg/mL, $p < 0.0001$, n = 6), while Aloin treatment at all doses (Aloin 20 mg/kg: 98.79 ± 8.35 pg/mL, $p < 0.0001$, n = 6; Aloin 40 mg/kg: 91.94 ± 10.71 pg/mL, $p < 0.0001$, n = 6; Aloin 80 mg/kg: 71.24 ± 4.77 pg/mL, $p < 0.0001$, n = 6) significantly reduced IL-6 concentrations compared to the EAP group. Finally, serum TNF-α levels were significantly higher in the EAP group compared to the NC group (EAP: 226.10 ± 15.94 pg/mL, NC: 133.10 ± 28.72 pg/mL, $p < 0.0001$, n = 6) and a significant reduction in TNF-α

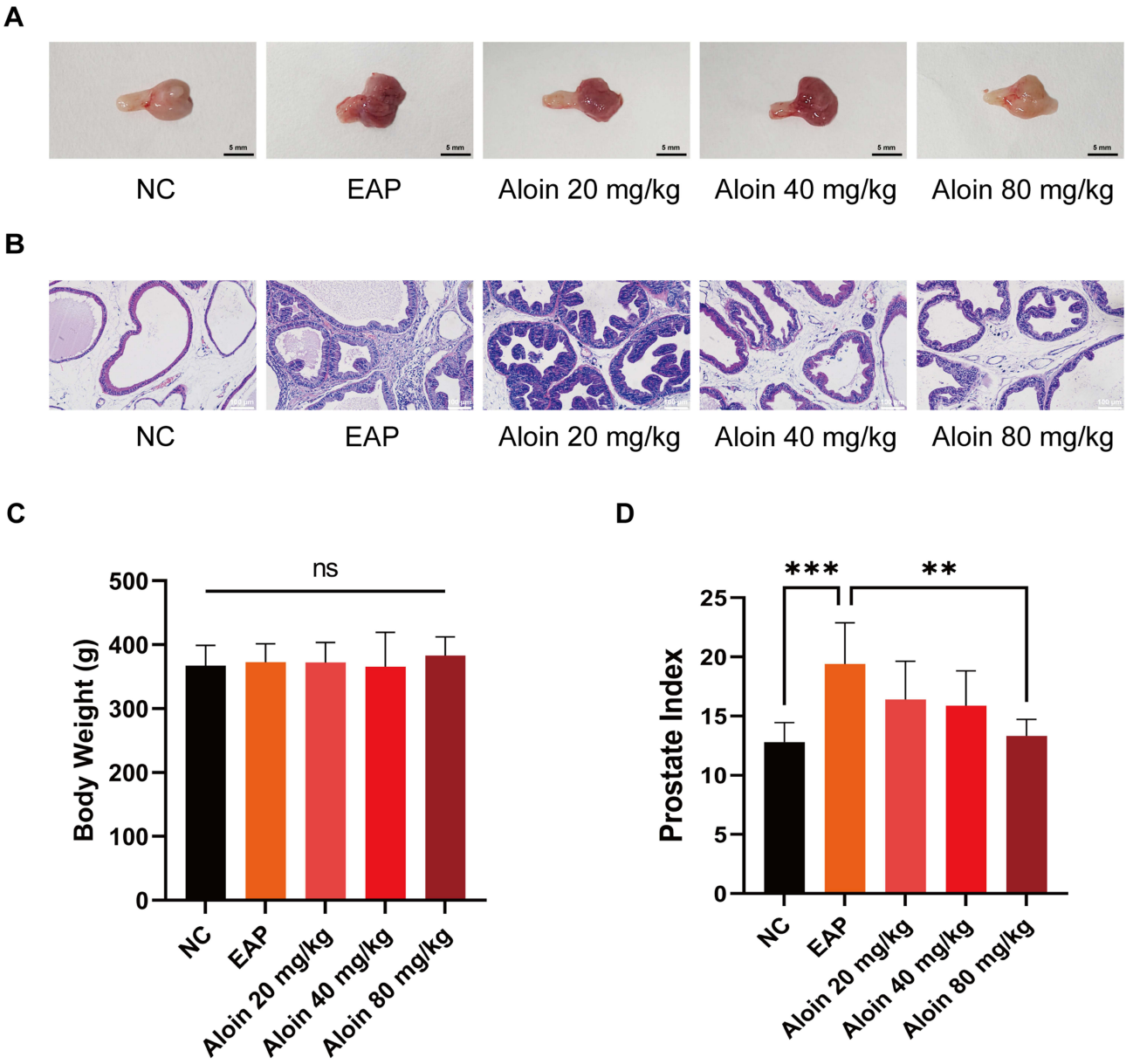

Figure 12 Gross and microscopic changes in prostate tissue. (**A**) Gross manifestation of prostate tissue in rats. Each photograph is representative of results obtained from 6 independent samples (n = 6). (**B**) H&E staining of the rat prostate tissue in different groups (magnification, × 200). Each photograph is representative of results obtained from 6 independent samples (n = 6). (**C**) Body weight in each group at the end of the experiment (n = 6). (**D**) The prostatic index of rats in each group at the end of the experiment (Prostate Index = Prostate Weight (mg) / Body Weight (g) × 10) (n = 6). Data are presented as mean ± SD; significance is denoted as $^{**}p < 0.01$, $^{***}p < 0.001$.

levels was observed only in the Aloin 80 mg/kg group (144.80 ± 36.68 pg/mL, $p < 0.0001$, n = 6), while no significant changes were noted at the 20 mg/kg or 40 mg/kg doses (Aloin 20 mg/kg: 200.20 ± 12.49 pg/mL, $p = 0.3844$, n = 6; Aloin 40 mg/kg: 195.70 ± 21.15 pg/mL, $p = 0.2352$, n = 6) (Figure 13G).

These findings suggest that Aloin treatment effectively reduces inflammatory infiltration and pro-inflammatory cytokine levels (IL-1β, IL-6, and TNF-α) in the prostate tissue of CP/CPPS rats.

Aloin Ameliorates Oxidative Stress Levels in Animal Models

IHC staining of rat prostate tissue revealed significantly higher levels of COX-2 and iNOS in the EAP group compared to the normal controls. Aloin treatment notably reduced the expression of COX-2 and iNOS in the prostate tissue (Figure 14A). Additionally, oxidative stress was evaluated using markers such as MDA, SOD, and CAT. The MDA

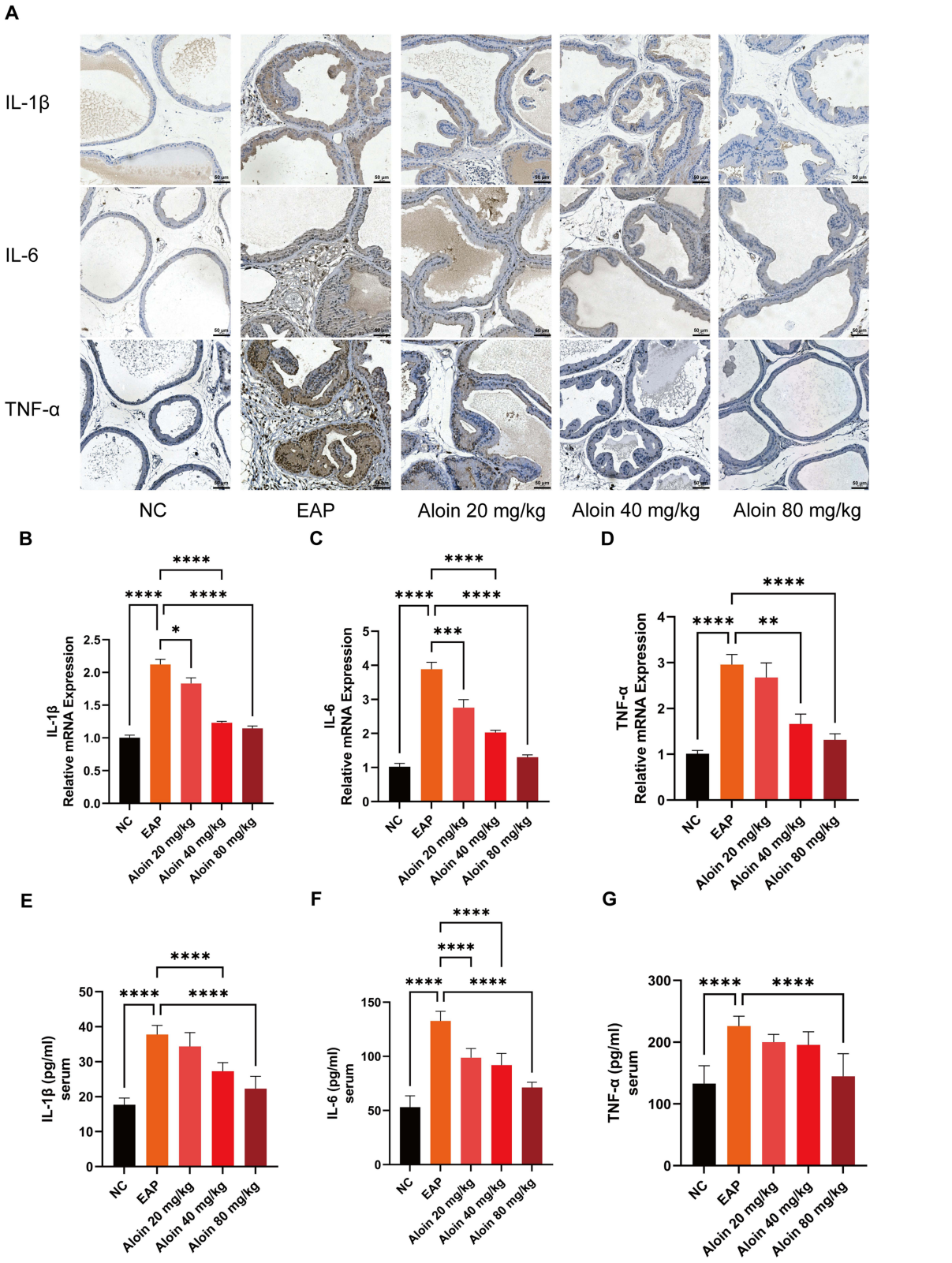

Figure 13 Expression of inflammatory factors in prostate tissue of rats in each group. (**A**) Representative immunohistochemical images of IL-1β, IL-6, and TNF-α in each group. Each photograph is representative of results obtained from 6 independent samples (n = 6). (**B**) The mRNA expression levels of IL-1β in prostate tissue (n = 6). (**C**) The mRNA expression levels of IL-6 in prostate tissue (n = 6). (**D**) The mRNA expression levels of TNF-α in prostate tissue (n = 6). (**E**) The expression levels of IL-1β in serum of rats in each group (n = 6). (**F**) The expression levels of IL-6 in serum of rats in each group (n = 6). (**G**) The expression levels of TNF-α in serum of rats in each group (n = 6). Data are presented as mean ± SD; significance is denoted as *p < 0.05, **p < 0.01, ***p < 0.001, ****p < 0.0001.

https://doi.org/10.2147/DDDT.S473678

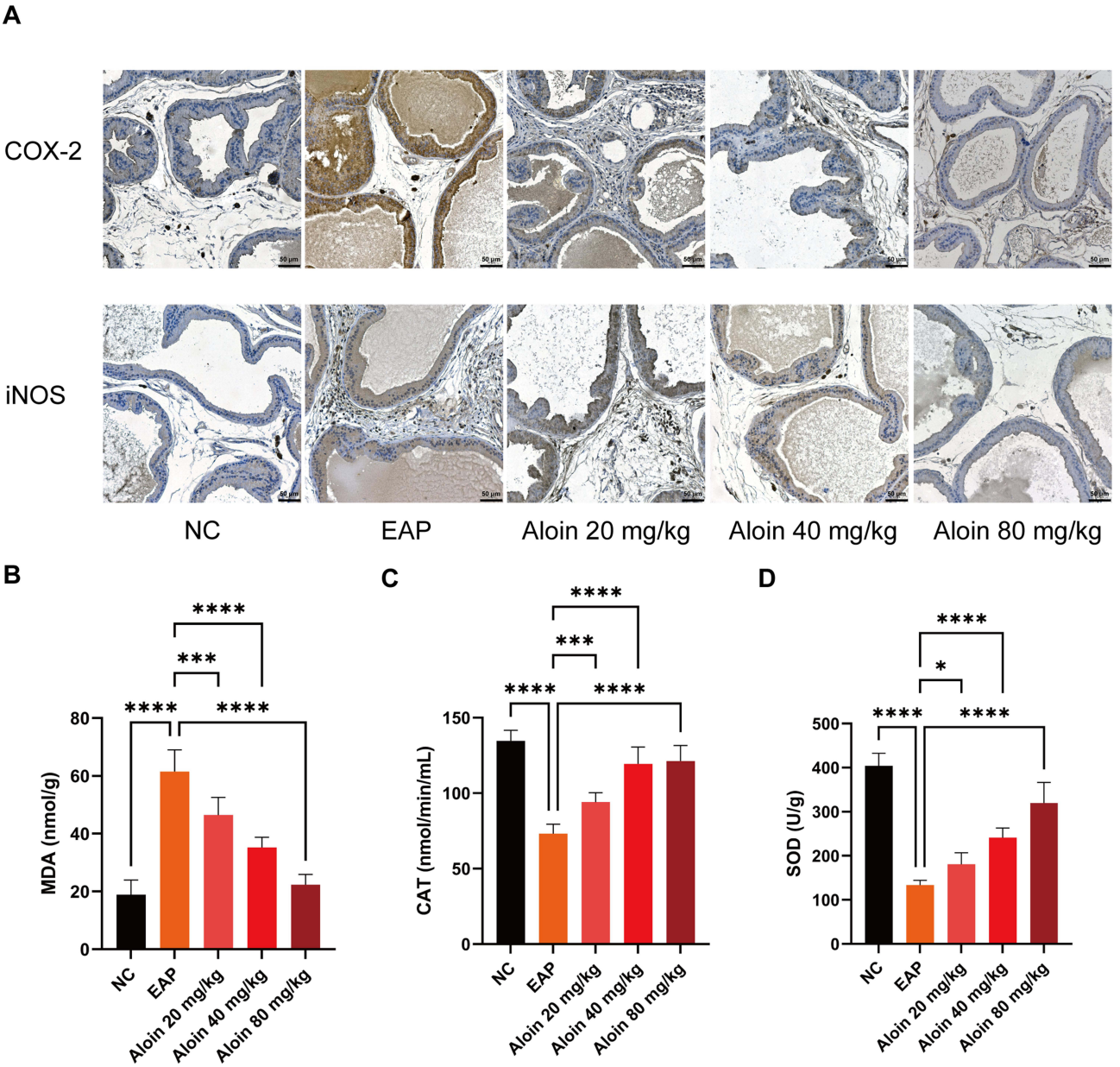

Figure 14 Expression of oxidative stress levels in each group of rats. (**A**) Representative immunohistochemical images of COX-2 and iNOS in each group. Each photograph is representative of results obtained from 6 independent samples (n = 6). (**B**) The MDA levels in prostate tissue of rats in each group (n = 6). (**C**) The CAT levels in prostate tissue of rats in each group (n = 6). (**D**) The SOD levels in prostate tissue of rats in each group (n = 6). Data are presented as mean ± SD; significance is denoted as *p < 0.05, ***p < 0.001, ****p < 0.0001.

levels were markedly elevated in the prostate tissue of the model group, while the activities of CAT and SOD were significantly reduced. Aloin treatment resulted in a substantial decrease in MDA levels and a significant increase in CAT and SOD levels compared to the EAP group, indicating a beneficial effect of Aloin on oxidative stress in the prostate tissue of CP/CPPS rats.

Specifically, the MDA level in the prostate tissue of the EAP group was significantly higher than that of the NC group (EAP: 61.49 ± 7.55 nmol/g, NC: 18.92 ± 5.07 nmol/g, $p < 0.0001$, n = 6). Treatment with Aloin (20 mg/kg, 40 mg/kg, 80 mg/kg) significantly reduced MDA levels compared to the EAP group (Aloin 20 mg/kg: 46.44 ± 6.11 nmol/g, $p = 0.0002$, n = 6; Aloin 40 mg/kg: 35.26 ± 3.53 nmol/g, $p < 0.0001$, n = 6; Aloin 80 mg/kg: 22.36 ± 3.53 nmol/g, $p < 0.0001$, n = 6) (Figure 14B). Similarly, the CAT levels in the EAP group were significantly decreased compared to the NC group (EAP: 73.15 ± 6.31 nmol/min/mL, NC: 134.7 ± 7.02 nmol/min/mL, $p < 0.0001$, n = 6), while the Aloin-treated groups showed a marked increase in CAT

levels (Aloin 20 mg/kg: 94.02 ± 6.25 nmol/min/mL, p = 0.0009, n = 6; Aloin 40 mg/kg: 119.5 ± 11.03 nmol/min/mL, p < 0.0001, n = 6; Aloin 80 mg/kg: 121.4 ± 10.22 nmol/min/mL, p < 0.0001, n = 6) (Figure 14C). Furthermore, SOD levels were significantly lower in the EAP group compared to the NC group (EAP: 133.4 ± 10.96 U/g, NC: 404.2 ± 28.33 U/g, p < 0.0001, n = 6). In contrast, the SOD levels were significantly elevated in the Aloin-treated groups (Aloin 20 mg/kg: 180.50 ± 26.21 U/g, p = 0.0338, n = 6; Aloin 40 mg/kg: 241.10 ± 22.11 U/g, p < 0.0001, n = 6; Aloin 80 mg/kg: 319.7 ± 46.82 U/g, p < 0.0001, n = 6) (Figure 14D). These findings suggest that Aloin treatment effectively mitigates oxidative stress in the prostate tissue of CP/CPPS rats.

mRNA Expression Validation of Core Targets Identified Through Network Pharmacology

The mRNA expression levels of the core target genes AKT1, EGFR, ESR1, HSP90AA1, and SRC in the prostate tissue of rats were further validated by qRT-PCR, following the network pharmacology screening. The expression level of AKT1 mRNA in prostate tissue was significantly higher in the EAP group compared to the NC group (NC: 1.000 ± 0.425; EAP: 5.235 ± 1.184; p < 0.0001, n = 6), while the expression levels in the Aloin 40 mg/kg and Aloin 80 mg/kg groups were significantly lower than in the EAP group (Aloin 40 mg/kg: 2.642 ± 0.763, p < 0.0001, n = 6; Aloin 80 mg/kg: 1.118 ± 0.285, p < 0.0001, n = 6), with no significant difference observed between the Aloin 20 mg/kg group and the EAP group (Aloin 20 mg/kg: 5.019 ± 1.030, p = 0.9725, n = 6) (Figure 15A). Compared to the NC group, the expression level of EGFR mRNA in the prostate tissue of the EAP group was significantly elevated (NC: 1.000 ± 0.436, EAP: 3.703 ± 1.231, p < 0.0001, n = 6), whereas the EGFR mRNA expression levels in the Aloin 20 mg/kg, Aloin 40 mg/kg, and Aloin 80 mg/kg groups were all significantly lower than those in the EAP group (Aloin 20 mg/kg: 2.351 ± 0.371, p = 0.0066, n = 6; Aloin 40 mg/kg: 1.461 ± 0.375, p < 0.0001, n = 6; Aloin 80 mg/kg: 1.191 ± 0.526, p < 0.0001, n = 6) (Figure 15B). The expression level of ESR1 mRNA in the prostate tissue of the EAP group was significantly decreased compared to the NC group (NC: 1.000 ± 0.218, EAP: 0.351 ± 0.088, p < 0.0001, n = 6), but was significantly increased in the Aloin 40 mg/kg and Aloin 80 mg/kg groups compared to the EAP group (Aloin 40 mg/kg: 0.713 ± 0.134, p = 0.0035, n = 6; Aloin 80 mg/kg: 0.968 ± 0.145, p < 0.0001, n = 6); in contrast, the increase in ESR1 mRNA expression in the Aloin 20 mg/kg group compared to the EAP group was not statistically significant (Aloin 20 mg/kg: 0.531 ± 0.215, p = 0.2172, n = 6) (Figure 15C). The expression level of HSP90AA1 mRNA in the prostate tissue of the EAP group was significantly higher than in the NC group (NC: 1.000 ± 0.081, EAP: 2.479 ± 0.176, p < 0.0001, n = 6); however, it was significantly reduced in the Aloin 40 mg/kg and Aloin 80 mg/kg groups compared to the EAP group, while the Aloin 20 mg/kg group showed no statistically significant difference in HSP90AA1 mRNA expression compared to the EAP group (Aloin 20 mg/kg: 2.314 ± 0.158, p = 0.1502, n = 6; Aloin 40 mg/kg: 1.957 ± 0.175, p < 0.0001, n = 6; Aloin 80 mg/kg: 0.994 ± 0.056, p < 0.0001, n = 6) (Figure 15D). Finally, the expression level of SRC mRNA in the prostate tissue of the EAP group was significantly higher than in the NC group (NC: 1.000 ± 0.178, EAP: 2.480 ± 0.313, p < 0.0001, n = 6), while the SRC mRNA expression levels in the Aloin 20 mg/kg, Aloin 40 mg/kg, and Aloin 80 mg/kg groups were all significantly lower than those in the EAP group (Aloin 20 mg/kg: 1.570 ± 0.243, p < 0.0001, n = 6; Aloin 40 mg/kg: 1.335 ± 0.412, p < 0.0001, n = 6; Aloin 80 mg/kg: 1.099 ± 0.248, p < 0.0001, n = 6) (Figure 15E). These results suggest that Aloin can significantly regulate the mRNA expression levels of target genes in the prostate tissues of rats in the EAP group, and these changes may contribute to the alleviation of CP/CPPS symptoms.

Discussion

CP/CPPS is classified as type III prostatitis in the NIH classification system, characterized by clinical symptoms including long-term pain and discomfort in the pelvic region, urinary symptoms such as dysuria, urinary urgency, urinary frequency, and urethral-related symptoms like a burning sensation.[1] Psychological symptoms, such as sexual dysfunction, depression, and anxiety, are also commonly associated with CP/CPPS.[13,14] The pathogenesis of CP/CPPS is not completely understood, and various factors are believed to contribute, making it a complex and multifactorial condition.[15] Despite the absence of detectable bacteria in clinical samples of CP/CPPS patients, inflammatory reactions still play a role in the condition.[16] Abnormal activities in the immune system, neural factors, and psychological factors are extensively studied in relation to CP/CPPS.[3,17,18] Current treatment strategies for CP/CPPS are frequently customized to alleviate symptoms based on patient

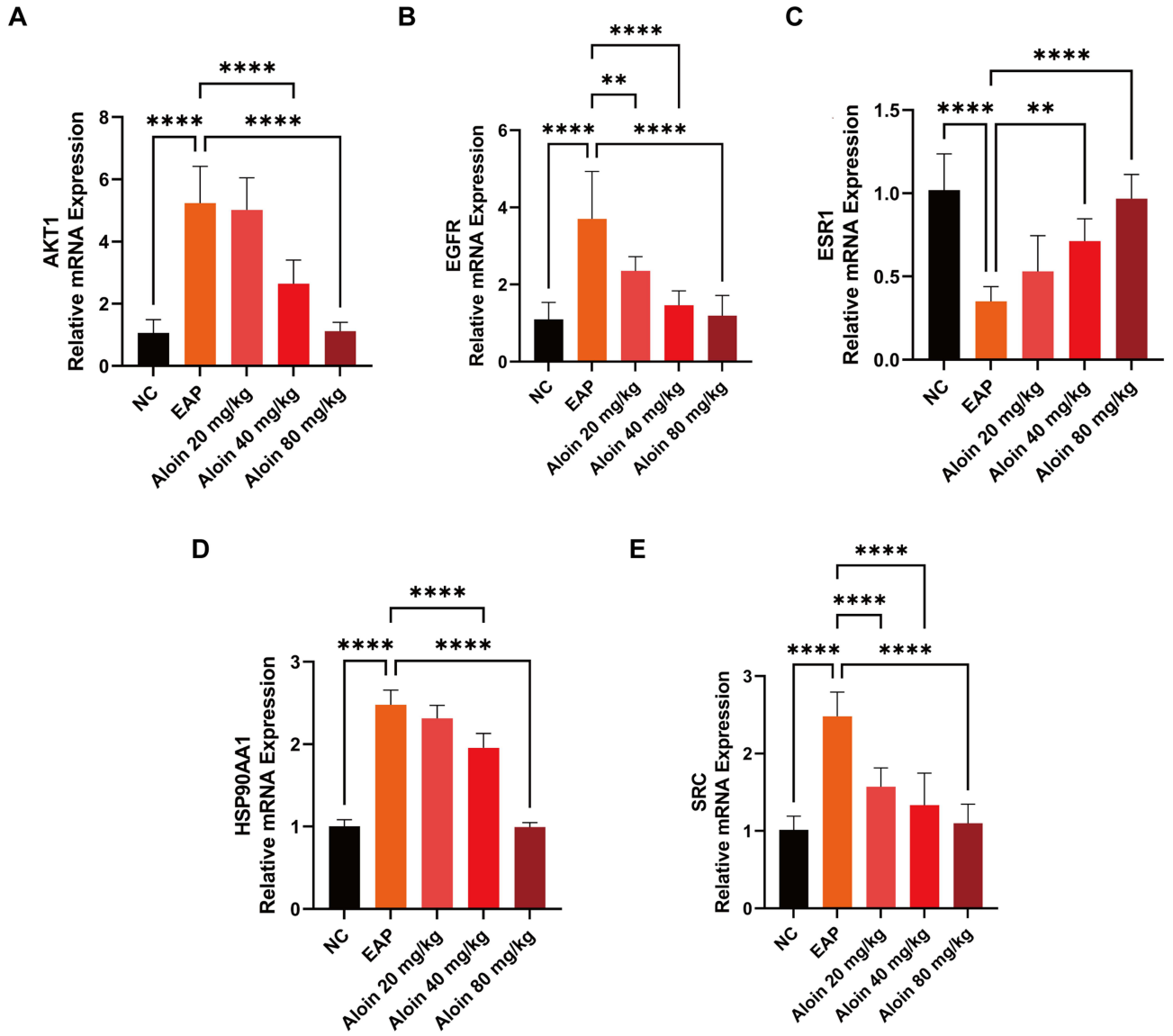

Figure 15 mRNA expression levels of core target genes in rat prostate tissue. (**A**) The mRNA expression levels of AKT1 (n = 6). (**B**) The mRNA expression levels of EGFR (n = 6). (**C**) The mRNA expression levels of ESR1 (n = 6). (**D**) The mRNA expression levels of HSP90AA1 (n = 6). (**E**) The mRNA expression levels of SRC (n = 6). Data are presented as mean ± SD. **p < 0.01, ****p < 0.0001.

presentation and examination results.[10,19,20] Hence, therapeutic interventions targeting symptoms and pathophysiological manifestations related to CP/CPPS may involve the use of drugs with potential therapeutic effects.

Aloin, derived from the natural plant Aloe vera, has been previously documented for its anti-inflammatory and antioxidant effects in in vivo or in vitro models of various diseases.[21–24] The mechanisms of action of Aloin in inflammatory diseases are diverse, including the modulation of inflammatory mediators and cell signaling pathways to alleviate inflammatory reactions.[25] Aloin is also thought to reduce oxidative stress by scavenging free radicals, protecting cells from oxidative damage.[26] Additionally, Aloin also exhibits various biological functions, including anticancer properties,[27–29] organ protection,[30–33] and antimicrobial effects.[34,35] Considering the clinical characteristics of CP/CPPS, disease features, and the demonstrated effects of Aloin in inflammatory diseases, we conducted this study to investigate the role of Aloin in alleviating CP/CPPS, examining clinical symptoms, pathology, and molecular biology aspects.

Network pharmacology is an interdisciplinary research approach that integrates computational biology, systems biology, and pharmacology. It explores the interrelationships among drugs, targets, and diseases by integrating large volumes of bioinformatics data and analyzing network structure and function. The primary objectives of network

pharmacology include unveiling the mechanisms of drug action, identifying novel drug targets, predicting drug side effects, and expediting the drug development process. Utilizing network pharmacology methods, researchers can analyze extensive biological data, construct drug-target-disease networks, pinpoint potential therapeutic targets, predict drug side effects, and offer a novel avenue for individualized medicine. The advancement of this field holds significant importance in advancing precision medicine and personalized drug therapy. Through network pharmacology, molecular docking, molecular dynamics simulation, and animal model experiments, we demonstrated for the first time that Aloin has an anti-inflammatory effect on CP/CPPS, and verified this effect through animal experiments.

The EAP animal model is presently acknowledged as a dependable in vivo model for CP/CPPS research. Referring to previous studies, we established an animal model of CP/CPPS through an intraprostatic injection of CFA.[36–38] Pain represents the primary clinical manifestation in individuals with CP/CPPS, significantly impacting the quality of life for affected patients.[39,40] Inflammatory infiltrates and dysregulation of inflammatory factors are hallmark features in the pathology of CP/CPPS.[41,42] The correlation between pathological pain and cytokines has been discussed.[43,44] Research suggests that individuals experiencing chronic pain exhibit abnormal levels of inflammatory cytokines, including TNF-α, IL-1β, and IL-6.[45] Our study revealed a reduction in pain threshold and an elevation in inflammatory factor levels in the prostate tissue and serum of CP/CPPS rats. This suggests a potential association between pain in CP/CPPS rats and increased inflammatory factors. Our results suggest Aloin intervention demonstrated effective alleviation of pain and reduction in inflammatory factor levels in CP/CPPS rats. The results of H&E staining and immunohistochemical staining suggested that Aloin could effectively alleviate the inflammatory cell infiltration and inflammatory factor levels in the prostate tissue of rats with the CP/CPPS model. These results suggest that Aloin can also exert its anti-inflammatory effects on CP/CPPS.

Oxidative stress also plays a role in the pathology of CP/CPPS.[7] Several studies have suggested a role for oxidative stress in clinical CP/CPPS patients.[46,47] Alterations in oxidative stress-related indices have also been reported in animal models of CP/CPPS.[48,49] In this study, we assessed tissue oxidative stress levels by examining indicators, including MDA, SOD, and CAT. MDA, a lipid peroxidation byproduct, serves as a biomarker for oxidative damage by altering the activity of biological membranes and impairing normal cellular function.[50] SOD serves as a vital defense mechanism by efficiently catalyzing the dismutation of superoxide radical anions, and converting them into hydrogen peroxide and water through enzymatic disproportionation reactions.[51] CAT, an essential antioxidant enzyme ubiquitously present in cells, plays a crucial role in the conversion of hydrogen peroxide to water.[52] Our study indicates that Aloin modulates oxidative stress in prostate tissue by influencing the expression levels of oxidative stress-related enzymes in the tissue. Additionally, these findings contribute to the understanding of Aloin's potential therapeutic role in managing oxidative stress in the context of prostatic conditions.

Our study identified five core targets that may play a critical role in the alleviation of CP/CPPS-related symptoms by Aloin, as revealed through a network pharmacology approach: AKT1, EGFR, ESR1, HSP90AA1, and SRC. AKT1 is a key signaling protein involved in various physiological processes, including cell survival, proliferation, and metabolism, and is a central component of the PI3K/AKT signaling pathway.[53] AKT1 is frequently upregulated or abnormally activated in numerous inflammation-related diseases.[49,54,55] As a transmembrane receptor, EGFR is a key member of the receptor tyrosine kinase family and is essential for cell proliferation, differentiation, and survival.[56] Overactivation of EGFR has been associated with inflammatory responses and oxidative stress.[57] EGFR plays a pivotal role in various inflammatory responses, particularly in the regulation of cytokines and growth factors.[57,58] ESR1 is a type of estrogen receptor that regulates the biological effects of estrogen in the body by binding to estrogen molecules, such as 17β-estradiol. Estrogens can exert anti-inflammatory and pain-alleviating effects by downregulating pro-inflammatory cytokines, including IL-1β, TNF-α, and IL-6.[59] Research has shown that in the sperm cells of patients with CP/CPPS, the methylation level of the ESR1 gene is significantly higher compared to that of the control group, and its expression is downregulated.[60] HSP90AA1 belongs to the heat shock protein 90α (HSP 90α) family and is involved in modulating biological processes like cellular oxidative stress and signal transduction. HSP90α is considered to be a key factor in inflammatory reactions and stress responses.[61] Inhibition of HSP90AA1 significantly reduces the levels of pro-inflammatory cytokines.[62,63] SRC, a non-receptor tyrosine protein kinase, regulates multiple cell signaling pathways, and its activation can lead to the release of inflammatory mediators.[64,65] SRC activation of glial cells promotes the release of inflammatory mediators, thereby exacerbating the oxidative stress response.[66] By assessing the mRNA expression levels of these targets in rat prostate tissues, we observed that in CP/CPPS rats, the mRNA levels of AKT1, EGFR, HSP90AA1, and SRC were upregulated, whereas ESR1 levels were downregulated. Furthermore, intervention with Aloin

partially reversed these changes. These findings suggest that Aloin may exert its anti-inflammatory and antioxidant effects in CP/CPPS by modulating the expression of these key targets.

In the present study, we found that Aloin could reduce inflammatory infiltration and oxidative stress levels while improving pain symptoms in CP/CPPS. Through network pharmacology, potential drug targets were explored, and experimental validation in animal models confirmed that Aloin reduces inflammatory cell infiltration, pain symptoms, and oxidative stress levels in the prostate tissues of CP/CPPS model rats. In the future, we will focus on the relevant targets suggested by network pharmacology and explore the specific mechanism of Aloin in treating CP/CPPS through more experiments.

Conclusion

According to the results of this study, Aloin may alleviate the painful symptoms of CP/CPPS by reducing the level of inflammation and improving oxidative stress in prostate tissue. Our study suggests that Aloin possesses potential pharmacological effects for the treatment of CP/CPPS, and its clinical effects and detailed mechanisms can be further explored in the future.

Abbreviations

CP/CPPS, Chronic Prostatitis/Chronic Pelvic Pain Syndrome; NIH, National Institutes of Health; TCMSP, Traditional Chinese Medicine Systems Pharmacology Database and Analysis Platform; PPI, Protein-Protein Interaction; GO, Gene Ontology; KEGG, Kyoto Encyclopedia of Genes and Genomes; BP, Biological Process; CC, Cellular Component; MF, Molecular Function; PDB, Protein Data Bank; AKT1, Protein Kinase B; EGFR, Epidermal Growth Factor Receptor; ESR1, Estrogen Receptor 1; HSP90AA1, Heat Shock Protein 90 Alpha Family Class A Member 1; SRC, Proto-Oncogene c-Src; RMSD, Root Mean Square Deviation; MD, Molecular dynamics; GAFF, Generalized Amber Force Field; RESP, Restrained Electrostatic Potential; TIP3P, Three-point transferable intermolecular potential; EM, Energy minimization; NVT, canonical ensemble; NPT, constant-pressure, constant-temperature; RMSF, Root Mean Square Fluctuation; Rg, Radius of Gyration; SASA, Solvent Accessible Surface Area; H-bonds, hydrogen bonds; SD, Sprague-Dawley; NC, Normal Control; EAP, Experimental Autoimmune Prostatitis; CFA, Complete Freund's Adjuvant; H&E, Hematoxylin and Eosin; IHC, immunohistochemistry; TNF-α, Tumor Necrosis Factor-α; IL-1β, Interleukin-1 beta; IL-6, Interleukin-6; COX-2, Cyclooxygenase-2; iNOS, Inducible Nitric Oxide Synthase; ELISA, Enzyme-linked immunosorbent assay; CAT, Catalase; SOD, Superoxide Dismutase; MDA, Malondialdehyde; qRT-PCR, Quantitative Real-Time Polymerase Chain Reaction; RNA, Ribonucleic Acid; Complementary Deoxyribonucleic Acid, cDNA; mRNA, Messenger Ribonucleic Acid; HSP90α, Heat Shock Protein 90α.

Ethics Approval

For human ethical compliance, this study was approved by the Institutional Medical Ethics Committee of the Second Hospital of Lanzhou University (Approval No. 2025A-035). All data used for the network pharmacology analysis were obtained from publicly available databases. The use of human data in our research complied with ethical guidelines of the Declaration of Helsinki. The data utilized in this research were anonymized and contained no personally identifiable information. For animal ethical compliance, the animal experiments were approved by the Animal Welfare and Ethics Committee of Lanzhou University Second Hospital (Approval No. D2023-127). We strictly managed and cared for the experimental animals by the Guidelines for the Welfare and Ethics of Experimental Animals (Ministry of Science and Technology of the People's Republic of China).

Funding

The research is financially supported by National Natural Science Foundation of China (Grant Number: 82160148).

Disclosure

The authors report no conflicts of interest in this work.

References

1. Krieger JN, Nyberg L, Nickel JC. NIH consensus definition and classification of prostatitis. *JAMA*. 1999;282(3):236–237. doi:10.1001/jama.282.3.236
2. Habermacher GM, Chason JT, Schaeffer AJ. Prostatitis/chronic pelvic pain syndrome. *Annu Rev Med*. 2006;57:195–206. doi:10.1146/annurev.med.57.011205.135654
3. Murphy SF, Schaeffer AJ, Thumbikat P. Immune mediators of chronic pelvic pain syndrome. *Nat Rev Urol*. 2014;11(5):259–269. doi:10.1038/nrurol.2014.63
4. Wang W, Naveed M, Baig MMFA, Abbas M, Xiaohui Z. Experimental rodent models of chronic prostatitis and evaluation criteria. *Biomed Pharmacother*. 2018;108:1894–1901. doi:10.1016/j.biopha.2018.10.010
5. Pontari MA. Etiology of chronic prostatitis/chronic pelvic pain syndrome: psychoimmunoneurendocrine dysfunction (PINE syndrome) or just a really bad infection? *World J Urol*. 2013;31(4):725–732. doi:10.1007/s00345-013-1061-z
6. Breser ML, Salazar FC, Rivero VE, Motrich RD. Immunological mechanisms underlying chronic pelvic pain and prostate inflammation in chronic pelvic pain syndrome. *Front Immunol*. 2017;8:898. doi:10.3389/fimmu.2017.00898
7. Ihsan AU, Khan FU, Khongorzul P, et al. Role of oxidative stress in pathology of chronic prostatitis/chronic pelvic pain syndrome and male infertility and antioxidants function in ameliorating oxidative stress. *Biomed Pharmacother*. 2018;106:714–723. doi:10.1016/j.biopha.2018.06.139
8. Franco JV, Turk T, Jung JH, et al. Non-pharmacological interventions for treating chronic prostatitis/chronic pelvic pain syndrome. *Cochrane Database Syst Rev*. 2018;5(5):CD012551. doi:10.1002/14651858.CD012551.pub3
9. Franco JVA, Turk T, Jung JH, et al. Pharmacological interventions for treating chronic prostatitis/chronic pelvic pain syndrome: a Cochrane systematic review. *BJU Int*. 2020;125(4):490–496. doi:10.1111/bju.14988
10. Polackwich AS, Shoskes DA. Chronic prostatitis/chronic pelvic pain syndrome: a review of evaluation and therapy. *Prostate Cancer Prostatic Dis*. 2016;19(2):132–138. doi:10.1038/pcan.2016.8
11. Yang Y, Wu -J-J, Xia J, et al. Can aloin develop to medicines or healthcare products? *Biomed Pharmacother*. 2022;153:113421. doi:10.1016/j.biopha.2022.113421
12. Xiao J, Chen S, Chen Y, Su J. The potential health benefits of aloin from genus Aloe. *Phytother Res*. 2022;36(2):873–890. doi:10.1002/ptr.7371
13. Ku JH, Kim SW, Paick J-S. Quality of life and psychological factors in chronic prostatitis/chronic pelvic pain syndrome. *Urology*. 2005;66(4):693–701. doi:10.1016/j.urology.2005.04.050
14. Pena VN, Engel N, Gabrielson AT, Rabinowitz MJ, Herati AS. Diagnostic and management strategies for patients with chronic prostatitis and chronic pelvic pain syndrome. *Drugs Aging*. 2021;38(10):845–886. doi:10.1007/s40266-021-00890-2
15. Schaeffer AJ. Etiology and management of chronic pelvic pain syndrome in men. *Urology*. 2004;63(3 Suppl 1):75–84. doi:10.1016/j.urology.2003.11.002
16. John H, Barghorn A, Funke G, et al. Noninflammatory chronic pelvic pain syndrome: immunological study in blood, ejaculate and prostate tissue. *Eur Urol*. 2001;39(1):72–78. doi:10.1159/000052415
17. Franco JV, Turk T, Jung JH, et al. Pharmacological interventions for treating chronic prostatitis/chronic pelvic pain syndrome. *Cochrane Database Syst Rev*. 2019;10(10):CD012552. doi:10.1002/14651858.CD012552.pub2
18. Franco JV, Turk T, Jung JH, et al. Non-pharmacological interventions for treating chronic prostatitis/chronic pelvic pain syndrome. *Cochrane Database Syst Rev*. 2018;1(1):CD012551. doi:10.1002/14651858.CD012551.pub2
19. Magistro G, Wagenlehner FME, Grabe M, Weidner W, Stief CG, Nickel JC. Contemporary management of chronic prostatitis/chronic pelvic pain syndrome. *Eur Urol*. 2016;69(2):286–297. doi:10.1016/j.eururo.2015.08.061
20. Cai T, Alidjanov J, Palagin I, Medina-Polo J, Nickel JC, Wagenlehner FME. Chronic prostatitis/chronic pelvic pain syndrome (CP/CPPS): look to the future. *Prostate Cancer Prostatic Dis*. 2024;27(2):239–241. doi:10.1038/s41391-023-00645-7
21. Jiang K, Guo S, Yang C, et al. Barbaloin protects against lipopolysaccharide (LPS)-induced acute lung injury by inhibiting the ROS-mediated PI3K/AKT/NF-κB pathway. *Int Immunopharmacol*. 2018;64:140–150. doi:10.1016/j.intimp.2018.08.023
22. Zhang C, Shao Z, Hu X, et al. Inhibition of PI3K/Akt/NF-κB signaling by Aloin for ameliorating the progression of osteoarthritis: in vitro and in vivo studies. *Int Immunopharmacol*. 2020;89(Pt B):107079. doi:10.1016/j.intimp.2020.107079
23. Jiang H, Shi G-F, Fang Y-X, et al. Aloin A prevents ulcerative colitis in mice by enhancing the intestinal barrier function via suppressing the notch signaling pathway. *Phytomedicine*. 2022;106:154403. doi:10.1016/j.phymed.2022.154403
24. Feng Y, Qiao H, Liu H, Wang J, Tang H. Exploration of the mechanism of aloin ameliorates of combined allergic rhinitis and asthma syndrome based on network pharmacology and experimental validation. *Front Pharmacol*. 2023;14:1218030. doi:10.3389/fphar.2023.1218030
25. Zhong J, Wang F, Wang Z, et al. Aloin attenuates cognitive impairment and inflammation induced by d-galactose via down-regulating ERK, p38 and NF-κB signaling pathway. *Int Immunopharmacol*. 2019;72:48–54. doi:10.1016/j.intimp.2019.03.050
26. Birari L, Wagh S, Patil KR, et al. Aloin alleviates doxorubicin-induced cardiotoxicity in rats by abrogating oxidative stress and pro-inflammatory cytokines. *Cancer Chemother Pharmacol*. 2020;86(3):419–426. doi:10.1007/s00280-020-04125-w
27. Sun R, Zhai R, Ma C, Miao W. Combination of aloin and metformin enhances the antitumor effect by inhibiting the growth and invasion and inducing apoptosis and autophagy in hepatocellular carcinoma through PI3K/AKT/mTOR pathway. *Cancer Med*. 2020;9(3):1141–1151. doi:10.1002/cam4.2723
28. Gao J, Yang S, Xie G, Pan J, Zhu F. Integrating network pharmacology and experimental verification to explore the pharmacological mechanisms of aloin against gastric cancer. *Drug Des Devel Ther*. 2022;16:1947–1961. doi:10.2147/DDDT.S360790
29. Jassi C, Kuo -W-W, Chang Y-C, et al. Aloin and CPT-11 combination activates miRNA-133b and downregulates IGF1R- PI3K/AKT/mTOR and MEK/ERK pathways to inhibit colorectal cancer progression. *Biomed Pharmacother*. 2023;169:115911. doi:10.1016/j.biopha.2023.115911
30. Zhang P, Liu X, Huang G, Bai C, Zhang Z, Li H. Barbaloin pretreatment attenuates myocardial ischemia-reperfusion injury via activation of AMPK. *Biochem Biophys Res Commun*. 2017;490(4):1215–1220. doi:10.1016/j.bbrc.2017.06.188
31. Du Y, Qian B, Gao L, et al. Aloin preconditioning attenuates hepatic ischemia/reperfusion injury via inhibiting TLR4/MyD88/NF-κB signal pathway in vivo and in vitro. *Oxid Med Cell Longev*. 2019;2019:3765898. doi:10.1155/2019/3765898
32. Lee W, Jeong G-S, Baek M-C, Ku S-K, Bae J-S. Renal protective effects of aloin in a mouse model of sepsis. *Food Chem Toxicol*. 2019;132:110651. doi:10.1016/j.fct.2019.110651

33. Lei J, Shen Y, Xv G, Di Z, Li Y, Li G. Aloin suppresses lipopolysaccharide-induced acute lung injury by inhibiting NLRP3/NF-κB via activation of SIRT1 in mice. *Immunopharmacol Immunotoxicol*. 2020;42(4):306–313. doi:10.1080/08923973.2020.1765373
34. Huang C-T, Hung C-Y, Hseih Y-C, et al. Effect of aloin on viral neuraminidase and hemagglutinin-specific T cell immunity in acute influenza. *Phytomedicine*. 2019;64:152904. doi:10.1016/j.phymed.2019.152904
35. Donkor A-M, Donkor MN, Kuubabongnaa N. Evaluation of anti-infective potencies of formulated aloin A ointment and aloin A isolated from aloe barbadensis miller. *BMC Chem*. 2020;14(1):8. doi:10.1186/s13065-020-0659-7
36. Lin L, Zhu B-P, Cai L. Therapeutic effect of melittin on a rat model of chronic prostatitis induced by complete freund's adjuvant. *Biomed Pharmacother*. 2017;90:921–927. doi:10.1016/j.biopha.2017.04.055
37. Meng L-Q, Yang F-Y, Wang M-S, et al. Quercetin protects against chronic prostatitis in rat model through NF-κB and MAPK signaling pathways. *Prostate*. 2018;78(11):790–800. doi:10.1002/pros.23536
38. Zhao Q, Yang F, Meng L, et al. Lycopene attenuates chronic prostatitis/chronic pelvic pain syndrome by inhibiting oxidative stress and inflammation via the interaction of NF-κB, MAPKs, and Nrf2 signaling pathways in rats. *Andrology*. 2020;8(3):747–755. doi:10.1111/andr.12747
39. Wagenlehner FME, van Till JWO, Magri V, et al. National institutes of health chronic prostatitis symptom index (NIH-CPSI) symptom evaluation in multinational cohorts of patients with chronic prostatitis/chronic pelvic pain syndrome. *Eur Urol*. 2013;63(5):953–959. doi:10.1016/j.eururo.2012.10.042
40. Zaidi N, Thomas D, Chughtai B. Management of chronic prostatitis (CP). *Curr Urol Rep*. 2018;19(11):88. doi:10.1007/s11934-018-0841-9
41. Alexander RB, Ponniah S, Hasday J, Hebel JR. Elevated levels of proinflammatory cytokines in the semen of patients with chronic prostatitis/chronic pelvic pain syndrome. *Urology*. 1998;52(5):744–749. doi:10.1016/S0090-4295(98)00390-2
42. Nadler RB, Koch AE, Calhoun EA, et al. IL-1beta and TNF-alpha in prostatic secretions are indicators in the evaluation of men with chronic prostatitis. *J Urol*. 2000;164(1):214–218. doi:10.1016/S0022-5347(05)67497-6
43. Gonçalves Dos Santos G, Delay L, Yaksh TL, Corr M. Neuraxial cytokines in pain states. *Front Immunol*. 2019;10:3061. doi:10.3389/fimmu.2019.03061
44. Vanderwall AG, Milligan ED. Cytokines in pain: harnessing endogenous anti-inflammatory signaling for improved pain management. *Front Immunol*. 2019;10:3009. doi:10.3389/fimmu.2019.03009
45. Zhang ZY, Zug C, Schluesener HJ. Sphingosine 1-phosphate receptor modulator FTY720 suppresses rat experimental autoimmune prostatitis. *Scand J Immunol*. 2011;73(6):546–553. doi:10.1111/j.1365-3083.2011.02528.x
46. Shahed AR, Shoskes DA. Oxidative stress in prostatic fluid of patients with chronic pelvic pain syndrome: correlation with gram positive bacterial growth and treatment response. *J Androl*. 2000;21(5):669–675. doi:10.1002/j.1939-4640.2000.tb02135.x
47. Kullisaar T, Türk S, Punab M, Mändar R. Oxidative stress--cause or consequence of male genital tract disorders? *Prostate*. 2012;72(9):977–983. doi:10.1002/pros.21502
48. Hu Y, Niu X, Wang G, Huang J, Liu M, Peng B. Chronic prostatitis/chronic pelvic pain syndrome impairs erectile function through increased endothelial dysfunction, oxidative stress, apoptosis, and corporal fibrosis in a rat model. *Andrology*. 2016;4(6):1209–1216. doi:10.1111/andr.12273
49. Feng B, Dong Z, Wang Y, et al. Li-ESWT treatment reduces inflammation, oxidative stress, and pain via the PI3K/AKT/FOXO1 pathway in autoimmune prostatitis rat models. *Andrology*. 2021;9(5):1593–1602. doi:10.1111/andr.13027
50. Kurutas EB. The importance of antioxidants which play the role in cellular response against oxidative/nitrosative stress: current state. *Nutr J*. 2016;15(1):71. doi:10.1186/s12937-016-0186-5
51. McCord JM, Edeas MA. SOD, Oxidative stress and human pathologies: a brief history and a future vision. *Biomed Pharmacother*. 2005;59(4):139–142. doi:10.1016/j.biopha.2005.03.005
52. Ali SS, Ahsan H, Zia MK, Siddiqui T, Khan FH. Understanding oxidants and antioxidants: classical team with new players. *J Food Biochem*. 2020;44(3):e13145. doi:10.1111/jfbc.13145
53. Liu R, Chen Y, Liu G, et al. PI3K/AKT pathway as a key link modulates the multidrug resistance of cancers. *Cell Death Dis*. 2020;11(9):797. doi:10.1038/s41419-020-02998-6
54. Yang J, Cheng M, Gu B, Wang J, Yan S, Xu D. CircRNA_09505 aggravates inflammation and joint damage in collagen-induced arthritis mice via miR-6089/AKT1/NF-κB axis. *Cell Death Dis*. 2020;11(10):833. doi:10.1038/s41419-020-03038-z
55. Yang T, Pan Q, Yue R, Liu G, Zhou Y. Daphnetin alleviates silica-induced pulmonary inflammation and fibrosis by regulating the PI3K/AKT1 signaling pathway in mice. *Int Immunopharmacol*. 2024;133:112004. doi:10.1016/j.intimp.2024.112004
56. Sabbah DA, Hajjo R, Sweidan K. Review on epidermal growth factor receptor (EGFR) structure, signaling pathways, interactions, and recent updates of EGFR inhibitors. *Curr Top Med Chem*. 2020;20(10):815–834. doi:10.2174/1568026620666200303123102
57. Wang Z, Zhu M, Li Q, et al. Lycorine ameliorates liver steatosis, oxidative stress, ferroptosis and intestinal homeostasis imbalance in MASLD mice. *Mol Med*. 2024;30(1):235. doi:10.1186/s10020-024-01003-6
58. Peng W, Xia Q, Zhang Y, Cao D, Zheng X. VEGF and EGFR signaling pathways are involved in the baicalein attenuation of OVA-induced airway inflammation and airway remodeling in mice. *Respir Res*. 2024;25(1):10. doi:10.1186/s12931-023-02637-6
59. Song -X-X, Jin L-Y, Li X-F, Luo Y, Yu B-W. Substance P mediates estrogen modulation proinflammatory cytokines release in intervertebral disc. *Inflammation*. 2021;44(2):506–517. doi:10.1007/s10753-020-01347-1
60. Nesheim N, Ellem S, Dansranjavin T, et al. Elevated seminal plasma estradiol and epigenetic inactivation of ESR1 and ESR2 is associated with CP/CPPS. *Oncotarget*. 2018;9(28):19623–19639. doi:10.18632/oncotarget.24714
61. Chen M, Su W, Chen F, Lai T, Liu Y, Yu D. Mechanisms underlying the therapeutic effects of 4-octyl itaconate in treating sepsis based on network pharmacology and molecular docking. *Front Genet*. 2022;13:1056405. doi:10.3389/fgene.2022.1056405
62. Xu Q, Liu C, Wang H, et al. Deciphering the impact of aggregated autophagy-related genes TUBA1B and HSP90AA1 on colorectal cancer evolution: a single-cell sequencing study of the tumor microenvironment. *Discov Oncol*. 2024;15(1):431. doi:10.1007/s12672-024-01322-4
63. Sim HB, Sang Son J, Gupta SK, et al. Development of Hsp90 inhibitor to regulate cytokine storms in excessive delayed- and acute inflammation. *Int Immunopharmacol*. 2024;137:112470. doi:10.1016/j.intimp.2024.112470
64. Byeon SE, Yi Y-S, Oh J, Yoo BC, Hong S, Cho JY. The role of Src kinase in macrophage-mediated inflammatory responses. *Mediators Inflamm*. 2012;2012:512926. doi:10.1155/2012/512926
65. Oh J, Yu T, Choi SJ, et al. Syk/Src pathway-targeted inhibition of skin inflammatory responses by carnosic acid. *Mediators Inflamm*. 2012;2012:781375. doi:10.1155/2012/781375
66. Li Y, Bao Y, Zheng H, Qin Y, Hua B. The nonreceptor protein tyrosine kinase Src participates in every step of cancer-induced bone pain. *Biomed Pharmacother*. 2021;141:111822. doi:10.1016/j.biopha.2021.111822